UC Berkeley
UC Berkeley Electronic Theses and Dissertations

Title
Representation and control in closed-loop brain-machine interface systems

Permalink
https://escholarship.org/uc/item/3x1645gm

Author
Moorman, Helene

Publication Date
2015

Peer reviewed|Thesis/dissertation

eScholarship.org Powered by the California Digital Library
University of California

Representation and control in closed-loop brain-machine interface systems

By

Helene Gunther Moorman

A dissertation submitted in partial satisfaction of the

requirements for the degree of

Doctor of Philosophy

in

Neuroscience

in the

Graduate Division

of the

University of California, Berkeley

Committee in Charge:

Professor Jose M. Carmena, Chair
Professor Robert Full
Professor Jack Gallant
Professor Richard Ivry

Spring 2015

© 2015 Copyright, Helene G. Moorman

All Rights Reserved

Abstract

Representation and control in closed-loop brain-machine interfaces

by

Helene Gunther Moorman

Doctor of Philosophy in Neuroscience

University of California, Berkeley

Professor Jose M. Carmena, Chair

Brain-machine interface (BMI) systems attempt to restore motor function lost due to injury or neurodegenerative disease by bypassing natural motor pathways and allowing direct neural control of a movement actuator. Such systems also hold promise for investigating questions about learning and motor control in a highly controlled and observable system. Here we utilize a BMI paradigm in which single unit neural spiking activity recorded from motor cortical areas in non-human primates is used to control the movement of a virtual on-screen movement actuator. A Kalman filter is used to decode intended movements from neural signals.

This work presents a newly designed set of hardware and software components for running BMI and other real-time control experiments that provides a flexible and extendible framework for synchronized data collection, stimulus presentation, and behavioral task control. This framework is Python based and soon to be released open source to the neuroscience community.

The feasibility of chronically recording from bimodal sensory neurons in macaque ventral pre-motor cortex (PMv) was tested. Sensory response properties of individual PMv neurons were measured through the presentation of visual and tactile stimuli on and around the primate subject's arm, while electrophysiology recordings were collected from the brain. The existence of "bimodal" PMv neurons with linked visual-tactile receptive fields was confirmed, and groundwork was laid for a future study observing changes in sensory responses in PMv neurons as skilled BMI control develops.

Inter-subject and inter-task variability in adaptation strategies to a novel feedback perturbation were explored in both natural motor control and BMI control contexts. The feedback perturbation involved the addition of a constant velocity vector to the control signal generated by the subject, which both improved and hampered performance on a target hitting task depending on the movement direction within the workspace. No consistent adaptation strategy across all subject-context combinations was observed,

indicating that neither a local nor a global adaptation strategy was consistently applied in the presence of such a perturbation.

Finally, a novel, virtual, kinematically redundant BMI actuator consisting of a 4-link kinematic chain was developed and tested. Macaque subjects were shown to be capable of actively controlling redundant degrees of freedom when available. Removing redundant degrees of freedom hindered performance on a control task. In contrast to previously published observations for kinematic control in the natural motor system, both task-relevant and null movements increased over time.

In summary, this work addresses a range of questions related to the design and implementation of BMI systems, as well as the control strategies employed by the brain during various types of BMI control. It lays the groundwork for several future studies to investigate the performance effects of characteristics such as PMv control and redundancy, and establishes new paradigms for studying learning in the context of BMI control and potentially motor control in general.

Acknowledgements

I would like to sincerely thank my advisor Dr. Jose Carmena for his support over the years and for convincing me that UC Berkeley was the right place for me. His scientific guidance and enthusiastic personality has made my time in the lab extremely pleasant and productive, and I'm grateful for the incredible amount freedom to pursue my academic interests he has granted me.

Thanks to my qualifying exam and thesis committees for their guidance and feedback throughout my studies. I am also grateful to the students, faculty, and staff of the Helen Wills Neuroscience Institute for being an incredibly smart and fun bunch of people and contributing to an outstanding academic experience. I would particularly like to thank my colleagues who entered the program with me in 2009, and who were my first friends in the Bay Area.

The past and current members of the Carmena lab have always been sources of stimulating discussion, commiseration, and fun. Our lab outings—camping, wine tasting, bar nights, and even a Washington DC limo tour—were amazing, and I hope to be lucky enough to experience the same level of camaraderie wherever my career takes me next. Amy and Aaron in particular welcomed me into the lab, trained me, and have been incredible sources of advice and feedback as well as amazing friends. I've missed them greatly for the last two years as they pursue their postdoctoral work across the country and across the world. Even more than their presence in the lab, I miss brunch and TV watching with Amy, and milkshakes and camping with Aaron. I've also been incredibly fortunate to get to collaborate with Suraj Gowda on several of the projects presented in this dissertation. He is an amazing scientist and problem solver, and his patience and sense of humor have made him a true pleasure to work with.

Mariana, Adam, and Chat, my housemates for 3 years, have made my time as a graduate student so much better. They welcomed me (and a cat) into their crowded house, shared their belongings with me, and made coming home something I always looked forward to. Our wine nights (they can strike at any time!), ski trips, family dinners, and board games made it so there was always fun to be had at the house. They are truly a second family to me and I look forward to being reunited someday in our castle estate.

Thanks to my parents Stephani Moorman and John Gunther who have cheered me on all my life and helped me to achieve my academic goals. Even throughout their own tough times, they were always there when I needed advice or help. Thanks also to my brother, Eric Gunther. Even though we don't get to see each other often, it's always fun to share stories about grad school and catch up on what's going on in our lives.

Finally, I would like to thank James Gao for being a constant source of love and support for the last 4.5 years. We share so much in common, and I love that we can have just as much fun talking about science as we can eating sushi or going bike camping. He is the best partner that I could ever ask for, and my graduate school experience would never have been the same without him.

Curriculum Vitae

Peer-reviewed articles and conference proceedings

Dangi S, Gowda S, Moorman HG, Orsborn AL, So K, Shanechi M, Carmena JM (2014) Continuous Closed-Loop Decoder Adaptation with a Recursive Maximum Likelihood Algorithm Allows for Rapid Performance Acquisition in Brain-Machine Interfaces. Neural Comput 26:1811–1839.

Dangi S*, Orsborn AL*, Moorman HG, Carmena JM (2013) Design and Analysis of Closed-Loop Decoder Adaptation Algorithms for Brain-Machine Interfaces. Neural Comput 25:1693–1731.

Gowda S, Orsborn AL, Overduin SA, Moorman HG, Carmena JM (2014) Designing Dynamical Properties of Brain-Machine Interfaces to Optimize Task-Specific Performance. IEEE Trans Neural Syst Rehabil Eng 22:911–920.

Moorman HG*, Gowda S*, Carmena JM (2015) Control of redundant kinematic degrees of freedom in a closed-loop brain-machine interface. In submission.

Orsborn AL*, Dangi S*, Moorman HG, Carmena JM (2011) Exploring time-scales of closed-loop decoder adaptation in brain-machine interfaces. Conf Proc Annu Int Conf IEEE Eng Med Biol Soc IEEE Eng Med Biol Soc Conf 2011:5436–5439.

Orsborn AL, Dangi S, Moorman HG, Carmena JM (2012) Closed-loop decoder adaptation on intermediate time-scales facilitates rapid BMI performance improvements independent of decoder initialization conditions. IEEE Trans Neural Syst Rehabil Eng 20:468–477.

Orsborn AL, Moorman HG, Overduin SA, Shanechi MM, Dimitrov DF, Carmena JM (2014) Closed-Loop Decoder Adaptation Shapes Neural Plasticity for Skillful Neuroprosthetic Control. Neuron 82:1380–1393.

Shanechi MM, Orsborn AO, Moorman HG, Gowda S, Carmena JM (2014) High-Performance Brain-Machine Interface Enabled by an Adaptive Optimal Feedback-Controlled Point Process Decoder. In the Proceedings of the 36th Annual International Conference of the IEEE EMBS on Neural Engineering.

Shanechi MM*, Orsborn AL*, Moorman HG*, Gowda S*, Dangi S, Carmena JM (2015) Rapid control and feedback rates in the sensorimotor pathway enhance neuroprosthetic control. In submission.

Authors contributed equally.

Conference abstracts

Moorman HG, Gowda S, Carmena JM (2014) Neural control strategies in a closed-loop brain-machine interface with a 4 degree of freedom redundant actuator. Society for Neuroscience annual meeting, Washington, D.C., November 2014.

Orsborn AL**,** Dangi S, Moorman HG, Carmena JM (2011) Closed-loop decoder adaptation on intermediate time-scales facilitates rapid BMI performance improvements independent of decoder initialization. Society for Neuroscience annual meeting, Washington, D.C., November 2011.

Orsborn AL, Dangi S, Moorman HG, Carmena JM (2012) Combining neural and decoder adaptation to improve brain-machine interface performance. Society for Neuroscience annual meeting, New Orleans, LA, October 2012.

Orsborn AL, Dangi S, Moorman HG Carmena JM (2012) Co-adaptive BMIs: Combining Neural and Decoder Plasticity. 4th annual Conference on Research in Encoding and Decoding Neural Ensembles (AREADNE), Santorini, Greece, June 2012.

Table of Contents

1 Introduction

1.1 Brain-machine interface (BMI) systems

Brain-machine interface (BMI) systems attempt to restore motor function lost due to injury or neurodegenerative disease by bypassing natural motor pathways and allowing direct neural control of some kind of movement actuator. The field of neural ensemble-controlled BMI has advanced rapidly in recent years, and impressive proofs of concept have been shown for rodents, non-human primates, and humans controlling a variety of virtual and physical actuators (Carmena, 2013). The mapping between the observed neural activity and the movement of the actuator is known as a decoder, and the design and optimization of the decoder is at the heart of BMI research. To a large degree, BMI research has tended to focus on biomimetic decoder design; that is, decoding algorithms that attempt to mimic the existing transform between brain activity and natural movements of the body, such as arm reaching movements. These biomimetic decoders are typically fitted from brain activity recorded during such natural movements (Taylor et al., 2002; Serruya et al., 2002; Carmena et al., 2003; Musallam et al., 2004; Santhanam et al., 2006; Ganguly and Carmena, 2009; O'Doherty et al., 2009, 2011; Shpigelman et al., 2009; Ethier et al., 2012; Gilja et al., 2012), and the quality of the decoding was assessed offline by comparing actual movement kinematics or dynamics with predictions of the same movements generated by the decoder.

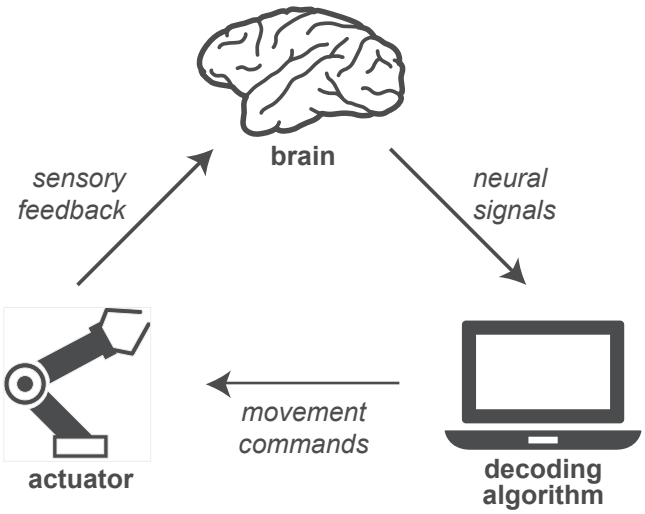

Figure 1.1: **Basic structure of closed-loop BMI system.** Signals from the user's brain are fed in to a decoding algorithm, which maps those signals to an appropriate movement command. Movement commands are sent to an actuator of some variety, which performs the movement. The loop is closed with sensory feedback (normally visual) back to the user, which enables learning and changes in strategy on the part of the user based on observed errors.

However, BMI systems are closed loop systems (see Figure 1.1). Motor commands from the brain (in the form of neural signals such as spikes, local field potentials, electrocorticography, or electroencephalography) are mapped to movements of the actuator (a computer, robot, prosthetic, or the subject's own muscles) through the decoding algorithm, and sensory feedback (usually visual) about the actuator's resulting movement is returned to the brain. Multiple groups have observed that biomimetic decoders do not always perform as well as predicted once implemented in closed-loop BMI systems (Koyama et al., 2009; Ganguly and Carmena, 2010; Cunningham et al., 2011). The existence of feedback in a closed-loop setting, combined with

imperfect control that generates error signals between the actuator movements and the subject's intended movements induce learning-related changes in the control signals generated by the brain. Several studies have demonstrated marked differences in the neural tuning properties observed during natural movement vs. BMI control (Taylor et al., 2002; Carmena et al., 2003; Moritz et al., 2008; Ganguly and Carmena, 2009), indicating that BMI-specific functional networks play a role in BMI control.

For these reasons, recent work has focused less on biomimetic approaches to decoder design and more on approaches that may use a biomimetic decoder as a starting point, but also take into account the brain's response to feedback during control. This may be accomplished either by providing a stable mapping over an extended period of time to allow the subject to learn (Ganguly and Carmena, 2009; Orsborn et al., 2014), or by using machine learning algorithms to optimize the mapping from neurons to movement online as a subject practices controlling the system (Taylor et al., 2002; Jarosiewicz et al., 2008; Velliste et al., 2008; Shpigelman et al., 2009; Vidaurre et al., 2010; Gilja et al., 2012; Hochberg et al., 2012; Orsborn et al., 2012).

1.2 BMI as a tool for studying the brain

While BMI technologies hold great promise for clinical applications, they also provide a unique environment in which to study academic areas of interest such as motor control, learning, and neuroplasticity. Because of the ability to observe and manipulate every part of the loop in Figure 1.1, experiments may be designed to test scientific questions for which too many uncontrolled variables exist in the natural motor pathway.

Some interesting demonstrations of this type of BMI study have been published. A number of operant conditioning studies by Fetz and colleagues have demonstrated that volitional control at the level of individual neurons in the brain is possible by linking the firing rate of a neuron directly to a reward (Fetz, 1969; Fetz and Finocchio, 1971; Fetz and Baker, 1973) or to another form of sensory feedback (Moritz et al., 2008; Moritz and Fetz, 2011) and showing that subjects are able to learn to volitionally modulate the firing rates of the neurons. Such experiments would not have been possible without the ability to establish a known causal link between the activity of individual neurons and the resulting feedback as is the case in paradigms that simply observe natural motor actions.

In a study by Jarosiewicz et al. (2008), the specificity of brain adaptation to a visual perturbation was studied by rotating the direction of select individual neurons' contribution to the decoded movement in a BMI system. Visual rotations have traditionally been used in motor control studies to learn about how error signals influence control, time scales of motor learning, and interference between motor skills (Krakauer and Mazzoni, 2011; Wolpert et al., 2011). Using a BMI framework to apply this type of manipulation at the level of the decoder instead of the actuator allowed the researchers to test several models of mechanisms by which the brain might accomplish the type of adaptation and error reduction observed in traditional behavioral studies.

Koralek et al. (2013) took advantage of the fact that the precise population of cells contributing to behavior actions in BMI are known in order to investigate temporal coordination between the striatum and individual cells in motor cortex. After establishing in an earlier study that corticostriatal plasticity plays a critical role in skill learning during BMI control (Koralek et al.,

2012), the researchers tested the specificity of corticostriatal coordination by measuring the coherence between activity in the striatum and the firing of individual cortical neurons as rodents learned to control a simple BMI system. They found that cells directly linked to behavior through the decoder developed higher levels of coherence with the striatum compared to neighboring non-BMI cells, indicating that corticostriatal networks are shaped by the relationship of individual cortical neurons to behavioral output. Similarly, Ganguly et al. (2011) examined differences over time between the activity of direct neurons (those that were part of the decoder) and neighboring indirect neurons as subjects learned BMI control and found that indirect neurons became modulated less over time than direct neurons.

In Chapter 3 we lay the groundwork for our own such basic science investigation by establishing a paradigm for chronically recording neural activity in macaque ventral pre-motor cortex, and probing the sensory representation embodied by the neurons in that area. In future work, we hope to use this paradigm to observe changes in that sensory representation as a result of learning skilled control of a novel actuator via a BMI system. Ultimately, these observations may contribute the understanding of how the brain uses feedback during active control to shape its sensory representation of the body during development or reorganization after injury.

1.3 Studying BMI-specific control

While certain questions about natural brain function may be suited to investigation using BMI paradigms, it must be acknowledged that many differences exist between BMI control and natural motor control. Because neuroscience currently lacks a complete understanding of how motor intentions are encoded in the brain, and because it is impossible to observe more than a small sample of the total brain activity at any given time with current experimental techniques, the exact way in which brain activity is mapped to movement in a BMI system is always unnatural to some degree. Additionally, while the natural motor pathway relies heavily on proprioceptive feedback from the body's joints and muscles, BMI systems must rely almost entirely on visual feedback, a property which may affect the way the brain solves the control problem.

Considering these facts, an understanding of the unique BMI-specific elements of control is an important factor for efforts to improve the design and function of BMI systems for clinical application. Several parts of this work attempt to explore control strategies that are specific to a BMI context. Chapter 4 compares behavioral adaptation to a unique feedback perturbation in BMI control and natural motor control. Chapter 5 examines control strategies in a kinematically redundant BMI system. The collaboration outlined in section 6.2 addresses the degree to which learning related changes occur in the brain in the presence of decoder adaptation in BMI. Finally, the collaboration outlined in section 6.4 investigates the effects of feedback and control rates on BMI control.

1.4 Chapter previews

In Chapter 2 we outline the design and configuration of a new fully integrated experimental data collection system for motor control, BMI, and other real time experiments. We describe a software ecosystem that is flexible and generalizable to many different unique laboratory setups, includes APIs for streaming from any data source and for implementing a wide range of

behavioral tasks and visual stimuli. We introduce a unified, web-based user interface for controlling experiments and accessing previously generated data. Finally, we outline the system's automated, efficient storage of data and metadata in a relational database which can be easily accessed and filtered.

In Chapter 3 we establish a paradigm for recording from macaque ventral pre-motor cortex using chronically implanted micro-wire arrays and for measuring responses to sensorimotor stimuli among neurons in this region. We present data confirming the existence of visual and somatosensory responses for neurons in ventral pre-motor cortex.

In Chapter 4 we examine adaptation to a novel type of sensory perturbation which can both assist and hinder movements depending on direction. We compare behavioral response to such a perturbation between a natural motor control context and several BMI control contexts, and observe inter-subject variability in adaptation strategies.

In Chapter 5 we present observations from a kinematically redundant BMI actuator in which the subject has direct neural control of more degrees of freedom than are required to perform the desired movements. We show evidence that the redundant degrees of freedom are incorporated into subjects' control strategy and that removing them hinders performance. We also examine the evolution of the subjects' control strategy over time and discuss our observations in the context of several models of redundancy resolution in the motor control literature.

In Chapter 6 we outline three collaborations that investigated questions of algorithm design and brain-decoder interactions in closed-loop BMI systems.

2 BMI3D real-time control and data collection system

To perform the studies discussed in the following chapters, the design and implementation of a robust, custom hardware and software system for data collection and closed-loop control was a necessary first step. This system had the following requirements:

- Stream data from and send commands to multiple hardware sources produced by different manufacturers (e.g. neural recording system, motion tracker, eye tracker, joystick, reward system, etc.) in real-time
- Display stimuli and closed-loop feedback to subjects in 2D or 3D
- Provide API for creation of stimuli and tasks
- Provide UI for configuring and running experiments
- Record and synchronize data from multiple sources
- Organize and provide access to data and metadata

In order to address these needs, a networked hardware system along with a custom Python-based software suite called BMI3D was developed. This system is generalizable to many different types of data acquisition hardware, data types, and experimental designs. Since its original inception, it has been utilized in four experimental rigs across two labs, with many individuals contributing to software and hardware improvement.

2.1 Hardware configuration

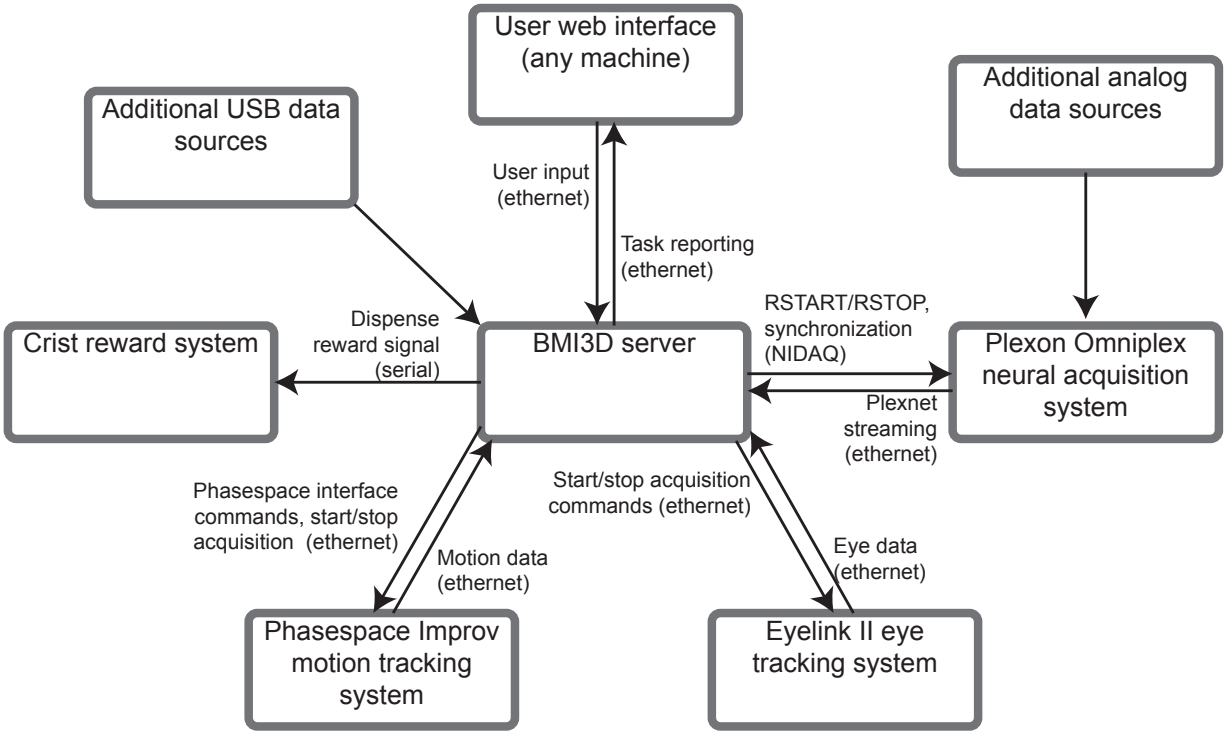

Figure 2.1: BMI3D hardware configuration diagram.

2.1.1 Server

The BMI3D server functions as the central hub of the system, sending and receiving information from all of the hardware components, controlling the stimulus display, and saving out the collected data. The server is a custom built desktop computer configured with the following specifications: Intel Quad Core i7 CPU, GeForce GTX 560 graphics card, 8 GB RAM, 120 GB solid state hard drive, two gigabit Ethernet adapters, two HDMI display outputs, National Instruments PC-6503 Data Acquisition (NIDAQ) card. It runs the Linux Ubuntu version 12.04 operating system. The server communicates with other hardware components via an 8-port gigabit network switch or via the NIDAQ card.

2.1.2 Stereo display

In order to enable experiments requiring 3D virtual environments, the BMI3D system includes a stereoscopic display optimized for non-human primate viewing (Figure 2.2). The display consists of two 23” 1080p computer monitors mounted parallel to each other and spaced 36” apart. In the center of the two monitors, two 4-inch square cold (reflective for visual light, transmissive for infrared light) mirrors are mounted at 90° to each other and at 45° to the monitors. The vertex edge where the mirrors come together is positioned at the exact midpoint of the horizontal, vertical, and depth dimensions of the space between the two monitors.

The subject is positioned at eye level to the vertical center of the mirrors, with the bridge of the nose at a distance of 1 cm or less from the mirror edges such that each of the two mirrors fill the field of view of one eye. When images are displayed on the monitors, the reflections are visible to the subject in the mirrors. If the same image is displayed on both monitors, the subject perceives a 2-D scene. A perception of depth may be introduced by adding disparity between the left and right images, allowing 3-D scenes to be displayed if the task so requires.

The display apparatus is mounted inside a custom-built framework of aluminum extrusions (80/20 Inc., Columbia City IN). The primate chair is wheeled inside the frame and secured with metal latches to prevent misalignment of the subject’s eyes from the mirrors during experiments.

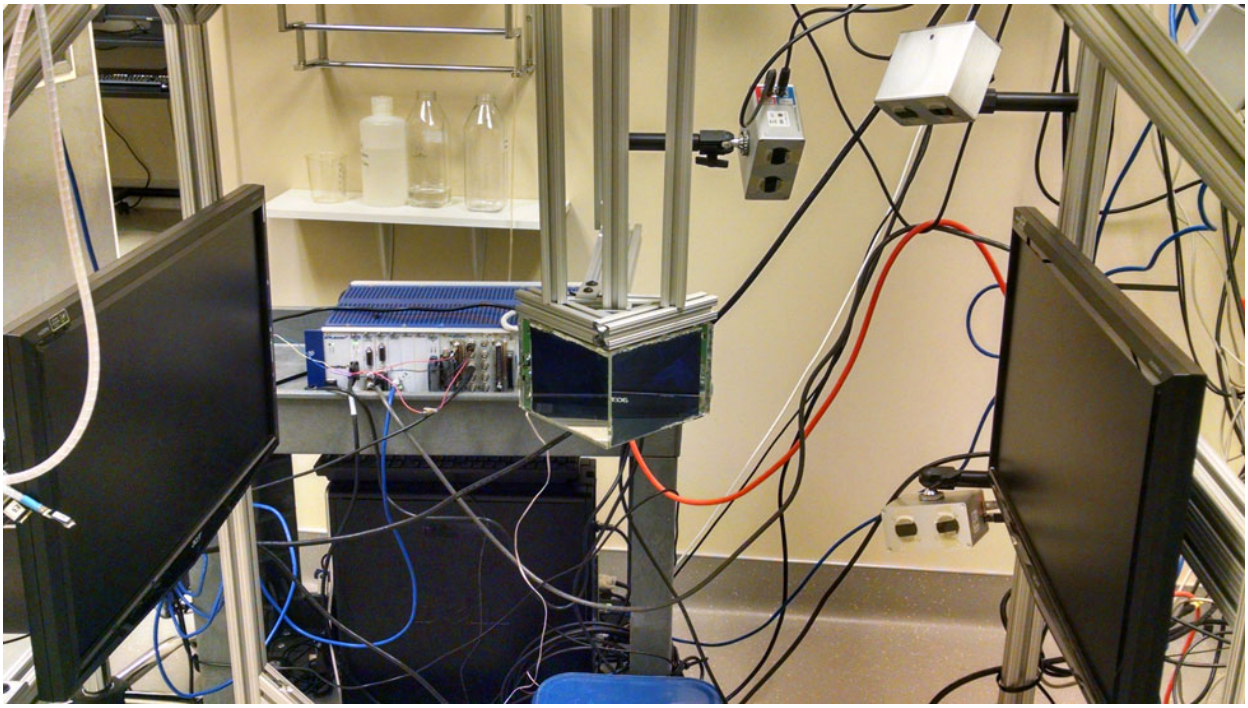

Figure 2.2: Stereo display. The angled mirrors at center reflect right and left eye images from the two monitors at either side. Motiontracking cameras (silver boxes) can also be observed in the upper right.

2.1.3 Neural data acquisition

Spike and local field potential data are recorded with an Omniplex neural acquisition system (Plexon Inc, Dallas, TX). This system includes a Windows 8 desktop computer along with the hardware required to collect, amplify, and digitize the neural signals. The Plexon computer streams real-time data to the BMI3D server via Ethernet, while the BMI3D server sends data synchronization signals and start/stop recording commands through the NIDAQ card to the Plexon system via an analog input on the Plexon chassis.

2.1.4 Motion tracking

Real-time 3D position data for up to 32 LED markers is collected using an Improv optical motion tracking system (Phasespace Inc, San Leandro, CA). The system includes 8 cameras which are mounted to the display frame such that the workspace around the subject's right arm and hand are well tracked. The Improv's computer streams position data to the server and receives start/stop commands via Ethernet.

2.1.5 Eye tracking

Eye tracking is performed with an Eyelink II system (SR Research Ltd, Mississauga, Ontario, Canada). The system's two infrared cameras along with a bright infrared light are mounted on a bar behind the cold mirrors, approximately 10 cm from the subject's eyes. The Eyelink II computer streams gaze data and receives start/stop commands from the BMI3D server via Ethernet.

2.1.6 Reward system

Liquid rewards are delivered to the subject using a 5-RLD-D1 reward system (Crist Instrument Company Inc). The reward system receives delivery commands from the server via an RS-232 serial interface.

2.1.7 Analog data sources

Additional analog data sources (e.g. electromyography, analog switches) may be added to the system by connecting them to the 32 auxiliary analog inputs on the Omniplex chassis, which in turn passes the data to the BMI3D server along with the neural data.

2.1.8 USB data sources

Additional data sources with a USB interface (e.g. joystick, touch sensor, etc.) may be added to the system by directly connecting them to the USB ports on the BMI3D server.

2.2 Software features

The BMI3D software package was developed primarily in Python and JavaScript. It forms a flexible, open framework for creating and running experiments, streaming data from any piece of hardware with an API available, and saving the data for analysis.

2.2.1 Data sources

Data sources refer to any source of data generated outside the BMI3D server while an experiment is running, such as neural data, eyetracking data, or motion data. Data from sources are streamed to the server in real time and may be accessed by the task during execution and/or written to file. Each source runs in its own process in order to accommodate different sampling rates.

A new source may be added to the system through the creation of a corresponding source class. Source classes inherit from the *DataSource* parent class and must contain *start(), run(), get(), read(), pause(),* and *stop()* functions, which interface with the data source using the manufacturer's API. Source data may be of any type or format that Python supports.

2.2.2 Stimulus display

Images related to the experiment are displayed for the subject using Pygame, a computer graphics Python library originally designed for use in creating video games. The stimulus environment consists of a collection of graphics objects which are built from a set of basic 3D shape primitives (e.g. rectangular solid, sphere, cone, plane). The graphics objects are instantiated by the task and passed to Pygame as 3D meshes, along with specifications such as screen location, size, color, and texture. Pygame handles the conversion of the mesh data to screen data, updating the monitors at a rate of 60 Hz.

2.2.3 Web interface

BMI3D contains a unified, web-based GUI written in JavaScript for the configuration and execution of experiments (Figure 2.3). The web interface may be run from any computer by pointing a browser to the BMI3D server's IP address, allowing flexibility of control and even remote access.

From the GUI, experimenters may select the task to be run and configure parameters or features. Convenient buttons allow starting, stopping, and pausing execution of the task as well as all data sources. The GUI allows notes to be added to a particular experiment entry before, during, or after execution. These notes are automatically saved to the database and can be retrieved or even searched at any time. There is also a console which displays real-time information about the task as it runs, such as the current state of the running task, the number of trials performed, the number of rewards received, etc. The information displayed in the console can be tailored to the specific task being run by adding a special *report()* function to the task class' definition. The console also displays error messages generated by the underlying Python software as a task runs, which may be used for debugging purposes.

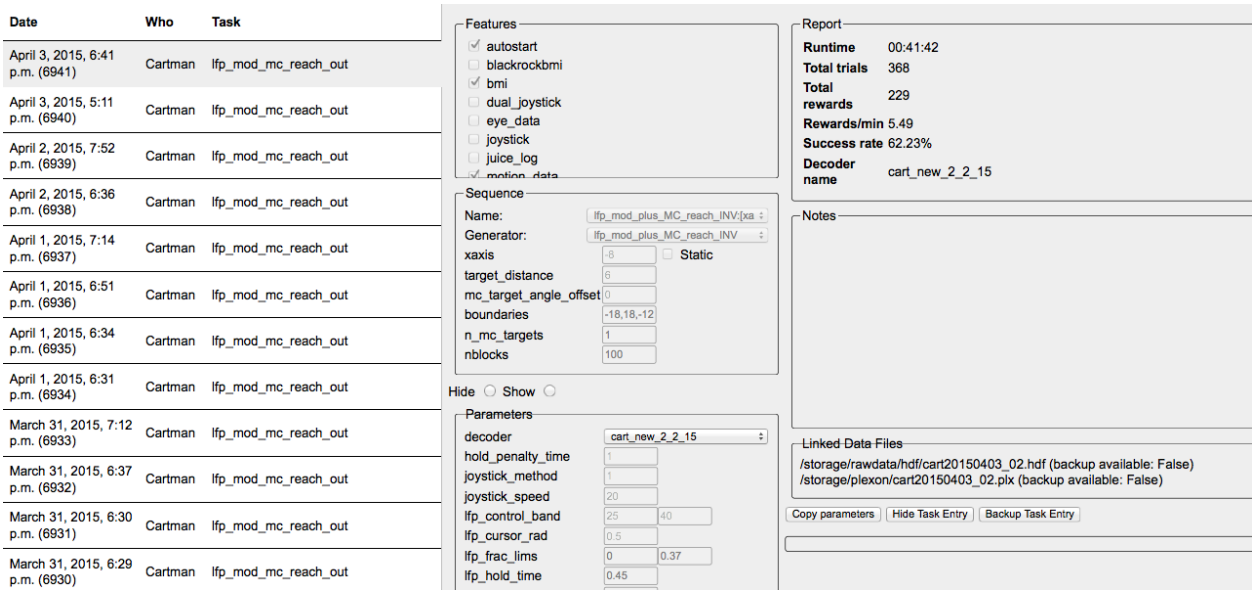

Figure 2.3: BMI3D web interface. Previous experimental sessions listed on the left may be viewed or copied. User configuration choices are specified in the middle column, and information about the task, data location, and notes are on the right.

2.2.4 Tasks

Tasks are Python classes which continuously receive source data and generate stimuli or other outputs. Task classes define the contingency structure, timing, and computation required for individual experiments. Tasks also specify which data is reported through the GUI during execution and which data is saved to file at the end.

Task classes inherit from the parent *Experiment* class, which contains a framework for parsing the individual task structure and starting and stopping execution. Tasks are run as finite state machines (FSMs), in which transitions between a set of pre-defined states are triggered by conditions that are tested periodically. A state transition model must be defined in each task class in the form of a Python dictionary called *status*. The *status* dictionary defines the possible transitions for every state and the corresponding trigger conditions (e.g. transition from a target state to a reward state if a cursor enters the target). Each transition condition is defined by a test

function which is repeated at 60 Hz and returns a boolean value; when a particular test function returns *True*, the corresponding state transition occurs.

Additionally, task classes contain a collection of functions that specify the actions to be performed before, during, and after each task state. These actions may include computation, calls to other functions or modules, changes to the displayed stimulus, communication with external elements such as a reward dispenser, or sending data to a file.

It is often beneficial to allow certain parameters (e.g. number of trials, target size, length of reward) to be configurable by the user for each execution of a particular task. This is accomplished through the specification of *Trait* variables within the task, the values of which are obtained from input fields in the web-based UI at each instantiation of a task.

2.2.5 Features

Features are special classes which provide functionality that is outside the scope of, and generally independent from, that of a task. An individual feature may be compatible with multiple tasks, and tasks may be executable with or without a particular feature. Unlike tasks, features are not mutually exclusive; multiple features may be active during the execution of a task (although not all features are compatible with all tasks). The primary uses for features are initializing data sources and writing to data files. Features are selected by the user through the GUI before starting a task. The BMI3D software then generates a hybrid class that inherits from all selected features in addition to the appropriate task class. By instantiating this class, the attributes and methods of the features are flexibly combined with those built in to the task.

2.2.6 Saving data

BMI3D provides the capability to save streamed data as well as data generated by the task itself in the versatile and efficient HDF5 file format. Variables to be recorded may be specified from within tasks or features by adding the variable name and data type to the *dtype* attribute in the initialization function. The current value of each variable is written to a new row of a table in the HDF5 file at 60 Hz (the rate at which the FSM of the task runs and the displays are refreshed). This guarantees that the sampling of each recorded variable is synchronized for later analysis. Metadata or static variables such as user-configured parameters may also be included in the HDF5 file as table attributes.

Data may also be streamed through a pipe from a source process to be written directly to the HDF5 file without being filtered through the task. This allows data that is sampled at a rate higher than 60 Hz to be recorded in the HDF5 file at its native sampling rate; however, the recorded samples are not synchronized with the data sent to the file by task in this case.

In addition to creating individual data files, BMI3D maintains a SQLite relational database for organization and access to previously recorded data. Each database entry contains a record of all associated data files for a particular execution of a task, as well as metadata such as parameter settings, recording date, subject data, task type and features used, summary statistics, and experimenter notes. Database entry creation is completely automated and greatly reduces the need for the experimenter to record experiment details by hand, which can easily lead to inaccuracies or omissions. The database can be queried, searched, or filtered either through the

BMI3D GUI or in Python using the Django web application framework. BMI3D includes a set of utility functions for extracting commonly-needed data elements from the database.

2.3 Conclusion

Overall, the BMI3D hardware/software suite provides a high level of both functionality and flexibility. It can be utilized by experimenters with a range of programming proficiencies. For experienced Python programmers it provides almost unlimited customization ability. It is version-controlled and maintained as a Git repository to allow continued development, and will eventually be released to the public with an open source license so that any researcher may take advantage of it or contribute to further development.

3 Sensorimotor encoding in ventral pre-motor cortex (PMv)

An early target for BMI control signal was primary motor cortex because of its role as the last cortical processing area before motor commands are sent to the spinal cord. Signals from M1 have been used successfully in a number of published BMI demonstrations (Chapin et al., 1999; Serruya et al., 2002; Carmena et al., 2003; Santhanam et al., 2006; Velliste et al., 2008; Jarosiewicz et al., 2008; Ganguly and Carmena, 2009; Ethier et al., 2012; Gilja et al., 2012; Hochberg et al., 2012; Orsborn et al., 2012, 2014; So et al., 2014; Wodlinger et al., 2015, and many more). However, multiple studies have demonstrated that other motor areas in addition to M1 can provide competent sources of control signal (Taylor et al., 2002; Carmena et al., 2003; Musallam et al., 2004; Ganguly and Carmena, 2009; Moritz and Fetz, 2011). One area of interest that has been explored little in the context of BMI control is ventral pre-motor cortex (PMv), which is located anterior to M1 and ventral to the dorsal pre-motor cortex (PMd). PMv projects heavily to M1 (Matelli et al., 1985).

PMv is identified as the ventral portion of Brodmann area 6 or Matelli et al's (1985) areas F5 and F4. Neurons in PMv exhibit responses to a variety of complex sensory and motor stimuli, particularly those related to the face, arm, and hand. These stimuli include reaching, grasping and orofacial movements (Rizzolatti et al., 1988), as well as the observation of such movements performed by others (i.e. "mirror neurons") (Caggiano et al., 2009). Multiple studies have also observed that approximately 30% of neurons in PMv display linked visual and tactile receptive fields (Rizzolatti et al., 1988; Fogassi et al., 1996; Graziano et al., 1997). These cells are known as "bimodal" neurons. These responses indicate that PMv may play a role in higher-level planning of movements involving the body's interaction with physical objects in the external environment, making it a potentially competent source of control signal for BMI devices.

The previously cited studies of PMv responses were performed using acute extracellular recordings. Although this methodology allows for a large total number of cells to be observed over the course of many recording sessions, it is not ideal for BMI because it limits observation to a small number of cells within a single session and does not allow the possibility of a stable, fixed ensemble of neurons with which the subject can practice control across multiple experimental sessions. Acute recordings also require significantly more preparation time before each session and create an increased infection risk in the subject because of the need for the brain to remain exposed after surgery. For these reasons, chronic multi-electrode arrays are the standard for BMI systems. Here we test the feasibility of implanting a chronic array in macaque PMv and attempt to confirm and characterize the types of neural responses observed in order to lay groundwork for future BMI studies involving chronic recording in this area.

3.1 Methods

3.1.1 Subjects

One male rhesus macaque monkey was used for this study. All procedures and animal care were conducted in compliance with the National Institutes of Health *Guide for the Care and Use of Laboratory Animals* and under the approval of UC Berkeley institutional review boards.

3.1.2 Surgery

A titanium headpost was surgically attached to the skull surface along the posterior midline using 16 titanium bone screws. In a second surgery 12 months later, the electrode arrays were implanted. The subject was anesthetized and the scalp and muscle incised along the midline to expose the skull. Craniotomies were performed over the pre-central motor cortical areas and arrays were placed bilaterally over the M1/PMd border and over PMv (4 total arrays, 384 total channels). The precise craniotomy positioning was based on coordinates from an atlas and anatomical landmarks. Each array was slowly lowered into the cortex by stereotax to a depth of 2.5-3 mm, targeting layer V pyramidal neurons. After array placement, the craniotomies were filled with surgical wax and the entire site was covered by a rigid cap of dental acrylic, leaving only the array connectors exposed.

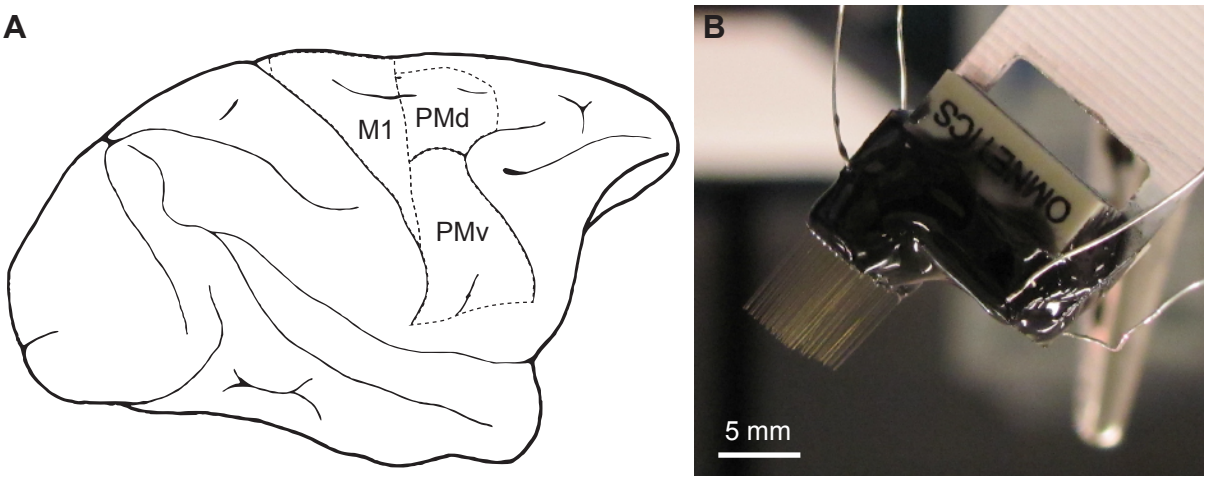

Figure 3.1: Recording array placement. A) Sagittal view of rhesus macaque cortical surface with primary motor cortex, dorsal pre-motor cortex, and ventral pre-motor cortex regions demarcated. B) A 128 channel microwire recording array before implantation.

3.1.3 Electrophysiology recording

Chronic, high-density arrays of 128 (M1) or 64 (PMv) microwire Teflon-coated tungsten electrodes (Figure 3.1B) with 35µm diameter and 500µm spacing (Innovative Neurophysiology, Durham, NC) were used to record single- and multi-unit neural activity as well as local field potentials (LFP). Voltage signals from the electrode channels were amplified and recorded using an OmniPlex data acquisition system (Plexon Inc, Dallas, TX). Spike sorting was performed online by the Omniplex system using principal component analysis and template matching.

3.1.4 Cursor control task

The subject was seated, head-fixed, in front of a stereo display in which circular targets and a circular cursor appeared. Movements of the right arm were tracked using an optical motion tracking system with an LED marker attached to the back of the hand (Phasespace Inc, San Leandro, CA), and the horizontal and vertical position of the hand was mapped to the position of the cursor within the plane of the display. The subject was trained to initiate trials by positioning the cursor in the center of the workspace. Targets appeared one at a time randomly around a

10cm radius circle and the subject was required to move the cursor to the target and hold at the target for 500ms. A juice reward was provided after each successful trial.

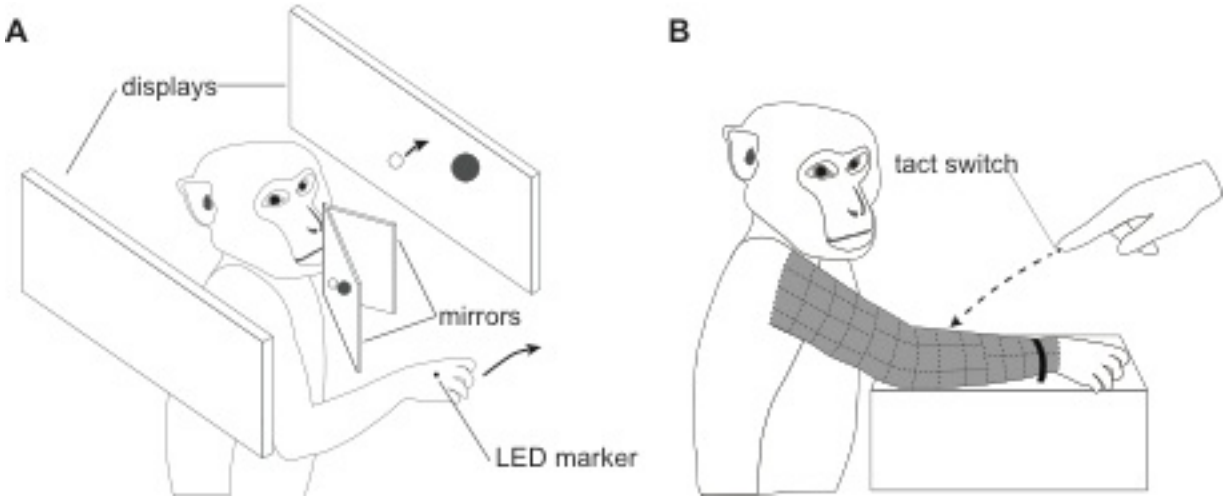

Figure 3.2: **Cursor control and sensory mapping tasks.** A) Cursor control task setup. The subject was seated in front of a stereo display, in which separate images were delivered to the left and right eyes by two angled mirrors reflecting displays located to the sides of the subject. Cursor and target locations appeared in the display. The cursor location reflected the subject's hand position which was tracked by an optical motion tracking system with an LED attached to the hand. B) Sensory stimulus task setup. The subject was seated with arm outstretched in front of him. A spandex sleeve with a numbered grid determined individual stimulus zones. Tactile and visual stimuli were delivered on or near the surface of the arm by the experimenter's hand. The timing of the stimuli was recorded by the activation of a small tact switch on the experimenter's finger. For some tactile stimuli sessions, the subject's eyes were covered by an opaque cloth.

3.1.5 Sensory receptive field mapping

For each recorded single or multiunit, the sensory receptive field consisted of the range of visual and tactile stimulation parameters that reliably induced a statistically significant increase in firing rate over baseline. The subject was seated, head-fixed, in the primate chair while visual and tactile stimuli were applied by the experimenter. Visual stimuli consisted of the movement of the tip of the experimenter's extended index finger toward the subject's right arm at a constant speed. The movement ceased just before making contact with the skin and the stimulus was immediately withdrawn. Tactile stimuli were generated in an identical fashion except that the experimenter continued moving toward the subject until making contact, and applied a small amount of pressure to the skin before withdrawing. For some sessions, the subject's eyes were covered to eliminate any visual component to the recorded responses.

The precise timing of the stimuli was recorded via a small tact-switch in the experimenter's possession. For visual stimuli, the experimenter manually activated the switch just before withdrawing her hand. For tactile stimuli, the switch was mounted on the tip of the finger so that it was depressed when contact was made with the subject.

To generate a range of controlled spatial locations for the stimuli, the subject wore a form-fitting sleeve stretching from the base of the fingers to the shoulder with a numbered 1-inch grid drawn on it. At the beginning of each trial, a location number was generated at random and the experimenter aimed the stimulus at the center of that zone on the subject's arm.

After each stimulus trial, the subject received a juice reward. If the subject ceased to remain still during a trial, the trial was excluded from analysis, no reward was given, and the experimenter waited until the movement subsided before continuing with the next trial.

3.1.6 Analysis of PMv unit responses

The spiking activity of 60 total neural units in PMv (single neurons or multi-units) was recorded during the cursor control and sensory mapping tasks. Not all units were present in all recording sessions, but individual units were often recorded for multiple sessions in a row. Since unit identity across sessions was difficult to determine with certainty, each recording session was analyzed separately. No significant differences in response were observed between sessions for the same unit.

A baseline mean firing rate and standard deviation for each unit was calculated for each session during a 5-10 minute period where the subject was sitting quietly and no task or stimulus was being presented. The response to a particular stimulus or movement was the z-scored firing rate during stimulus presentation or movement. To calculate changes in firing rate over time, a 50ms sliding window was used.

3.2 Results

3.2.1 Neural response to arm movement

PMv units exhibited arm movement-related activity and direction tuning during the cursor control task. Tuning curves for six representative units from one recording session are plotted in Figure 3.3A. Consistent with previous studies of motor cortical unit direction tuning, approximately cosine-shaped tuning patterns were observed. The time-varying activation for movements in the preferred direction, averaged across units during the same session, is shown in Figure 3.3B. Neural activation within trials increased above baseline during movements to the targets, and the activation peaked 300-400 ms after the appearance of the go cue.

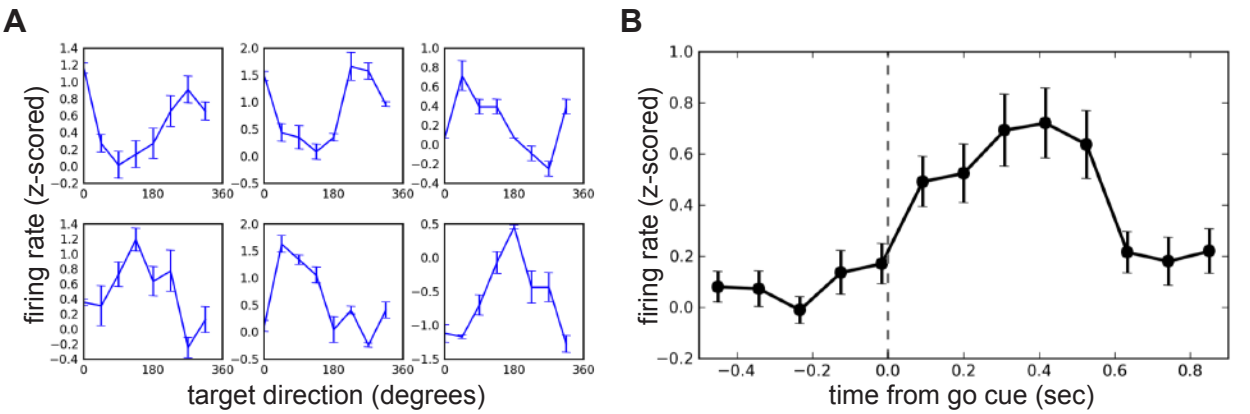

Figure 3.3: PMv unit responses to arm movements. A) Tuning curves for six representative PMv units. Average normalized firing rate was calculated for movements to targets in each of the eight directions. Error bars denote standard error. B) Time course of activation during movements to targets, averaged across trials and units. Only trials for the preferred target direction were included for each of the units. Error bars denote standard error.

3.2.2 Sensory mapping

On average, PMv units increased their firing rate over baseline when sensory stimuli were applied to the arm. Peak responses to tactile stimuli occurred 100-300 ms after skin contact, while peak responses to visual stimuli occurred 100-400 ms before the stimulus reached the end of its trajectory at the closest point to the subject's body (Figure 3.4A). The magnitude of visual and tactile responses for individual units was correlated, with a majority of units exhibiting stronger responses to tactile stimuli than to visual stimuli (Figure 3.4B).

Location-specific responses along the arm varied across the population of units, with most showing no quantifiable spatial pattern. Qualitatively, a few units exhibited an observable response gradient. The spatial response patterns for both types of stimuli are plotted for two such example units in Figure 3.4C.

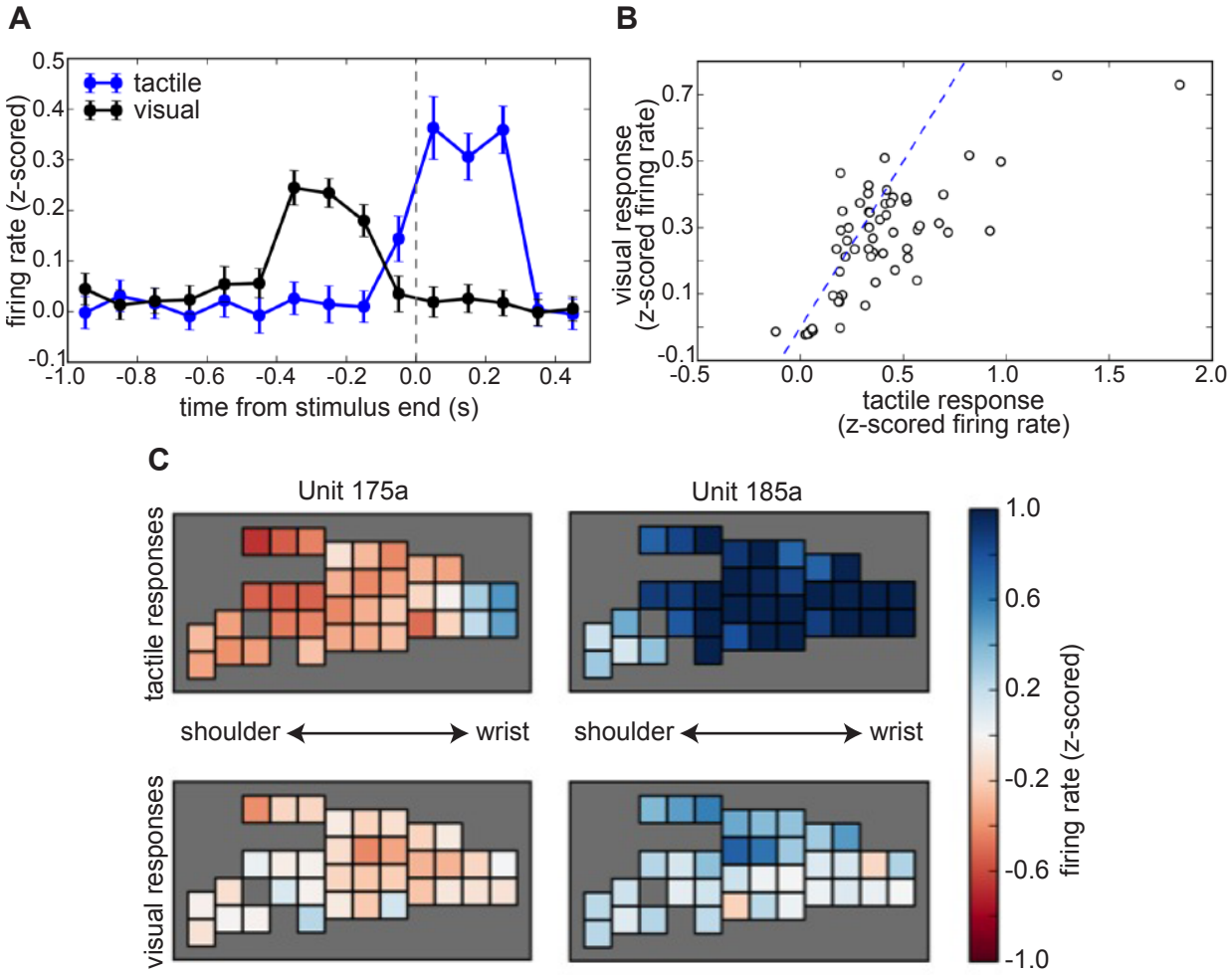

Figure 3.4: PMv unit responses to sensory stimulation. A) Average time-varying response to preferred stimulus location across 60 recorded PMv units during tactile and visual stimulus trials. Time 0.0 represents the time that the stimulus made contact with the subject's skin for tactile trials, and the time that the stimulus reached the point closest to the subject's skin for visual trials. Error bars denote standard error. B) Summary of magnitude of response to preferred tactile vs. preferred visual stimulus location for all 60 recorded PMv units. Responses to the two modalities within the population were correlated. A majority of recorded units exhibited stronger responses to tactile stimuli than to visual stimuli (points below unity line). C) Response of two example PMv units to tactile and visual stimulation at different spatial locations on the arm, averaged across 10 trials for each location. Each colored square represents one of the numbered zones on the subject's sleeve. Gray indicates regions where no data was collected.

3.3 Discussion

In this study, neurons in PMv were found to increase their firing rate in response to arm movements as well as tactile and visual stimuli around the arm. These findings agree with those previously published studies of PMv in which responses were measured with acute recording methods, indicating successful targeting of our implanted arrays to the intended region of cortex. The precise spatial structure of the receptive fields observed previously was generally not reproduced in our data. This may be related to the fact that our observations were gathered while

the subject was awake instead of anaesthetized or because we did not require fixation during our stimuli.

The presence of arm-movement induced responses observed in PMv units supports the possibility of this area being successfully used as a source of control signal in BMI systems. In future studies, this possibility should be tested, and the richness of the control signal should be compared to that of M1 and other motor cortical areas.

Bimodal sensory PMv neurons respond with increased firing rate to both tactile and visual stimuli on or near a particular location on the skin, most frequently on the hand, arm, or face. The response is not generally influenced by spatial location, body position, or gaze direction (Fogassi et al., 1996; Graziano et al., 1997). Since area PMv also contains neurons that are strongly active during complex reaching and grasping movement, one likely function of bimodal neurons in this area is the coordination of visually-guided activities such as feeding and climbing. Because these cells exhibit the unique property of responding to a purely visual stimulus only in close proximity to the body, observing their activity during the process of learning BMI control may represent an interesting opportunity to measure the degree to which a controlled real or virtual object is cortically represented as an extension of the body.

Evidence from previous studies suggests that the experience of a causal association between motor output and end effector response can alter or induce a neural representation of the end effector. Learning a new motor skill increases both motor (Kleim et al., 1998) and somatosensory (Hlustík et al., 2004) cortical representation of the body part being used. It can also induce long-term potentiation (LTP) (Rioult-Pedotti et al., 2000) and changes in dendritic spine width (Kleim et al., 2004) in motor cortex. Receptive fields of bimodal cells in lateral intraparietal area (LIP) can encompass hand tools (Iriki et al., 1996) and virtual representations of the natural arm (Iriki et al. 2001). These effects however, are only apparent after a moderate to high level of skill in controlling the end effector has been attained, implying that these changes do not occur instantaneously, but through learning with feedback.

In addition to evidence of broad learning-induced changes in cortical representations, several studies have shown that although the brain contains an innate and stable perceptual representation of a "normal" body, that representation may be altered to some degree by recent sensory experience (Carruthers, 2008). Perception of supernumerary limbs has been reported in humans after damage to the brain (Hari et al., 1998), and also as an illusion (Ehrsson, 2009). Perception of replacement of a limb with fake or virtual limb has been reported in humans with the "rubber hand" illusion (Botvinick and Cohen, 1998; Ehrsson et al., 2004; Slater et al., 2008; Sanchez-Vives et al., 2010). Sensory integration (feedback) is necessary for the perception of ownership of an external limb, and the perception is weaker or nonexistent for objects that do not look corporeal (Tsakiris et al., 2010).

In light of these studies, an important future direction of this work will be to observe possible changes in the sensory receptive fields of PMv units over time as a subject learns skilled control of a BMI using signals from a separate cortical region (such as M1). Such changes may provide insight into the brain's process of incorporating a prosthetic actuator into its cortical representation of the body. Specifically, we would like to test the hypothesis that PMv units will

start out exhibiting no response to visual stimuli around the BMI-controlled prosthetic (e.g. a virtual or robotic limb), but as control improves, sensory responses akin to those observed for the natural arm will develop for the prosthetic.

4 Adaptation to a constant velocity perturbation: a comparison across tasks

4.1 Background

Sensory feedback plays an important role in the learning of motor skills. Many researchers have attempted to study details of motor control by perturbing feedback during a motor task and observing the types of errors produced and the ways in which the system adapts to those errors over time (Krakauer and Mazzoni, 2011; Wolpert et al., 2011). For example in (Krakauer et al., 2000), human subjects were asked to make radial reaching movements with a robotic manipulandum. Perturbations to the feedback including a rotation of the hand position shown to the subjects were applied, causing the subjects to produce predictably stereotyped, curved trajectories. With practice, the magnitude of the perturbation's effect decreased, until subjects eventually fully adapted and produced straight-line trajectories like they had before the perturbation. When the perturbation was removed, subjects produced errors in the opposite direction, which were also gradually washed out with practice. This work was used to support the existence of an "internal model" in the motor system, which serves to predict the outcome of a motor command and may be modified based on the types of errors observed during practice.

More recently, a similar perturbation-adaptation paradigm has been adapted for use in brain-machine interface (BMI) studies, which are a promising tool for studying motor control because they allow observation of a known and controllable mapping between cortical output and actuator movement. These studies allow researchers to observe the effects of perturbations on the level of individual neurons, as in (Jarosiewicz et al., 2008) in which the firing rate of a small ensemble of motor cortical neurons in a non-human primate was mapped to cursor movement on a computer. Once the subject learned the mapping, the researchers rotated the direction of the contribution of individual neurons in the mapping and were able to observe the strategy with which the brain altered the activity of the ensemble to compensate for the resulting errors. This type of manipulation would not have been possible in a task involving natural motor movement because of the inability to identify all involved neurons and observe their activity.

Generally, perturbations in these types of experiments are designed to produce errors that the subject is motivated to correct, such as longer or less straight trajectories, slower movements, inaccurate targeting, etc. The perturbations chosen are also generally consistent in the type of effect across the workspace, e.g. a rotational perturbation causes an angular displacement of the same amount regardless of the direction of movement.

Little is known about how the motor system responds to feedback perturbations which produce a combination of disruptive and assistive effects depending on movement direction. In order to maximize performance, the optimal compensation strategy under such conditions would be a "local" adaptation strategy, in which the perturbation is counteracted for directions in which it is disruptive, but not for directions in which it is neutral or beneficial. Previous work has shown that human subjects making reaching movements can learn to compensate for two opposing dynamic force field perturbations if the movements (or visual feedback about the movements) under each force field occur in different regions of the workspace (Howard et al., 2013). Similarly, opposing visuomotor rotations can be learned when associated with spatially distinct

movement trajectories (Crossley et al., 2015). This evidence indicates that the brain is capable of compensating to perturbations a spatially-specific way, as opposed to a more "global" compensation strategy that is applied across all directions.

In this study we applied a unique perturbation to the visual feedback of a velocity-control movement task by adding a constant vector to all velocity commands generated by the subjects. This velocity perturbation improved (decreased) the movement time to some targets and worsened (increased) the movement time to others. The effects of the perturbation were tested for three non-human primate subjects under both a natural motor control condition and two BMI control conditions. Our aims were to 1) observe the type of adaptation strategy employed during a natural motor control task for this perturbation and 2) compare the type of adaptation observed during a BMI control task to the natural motor control task to determine whether they are consistent. A variety of different compensation strategies were observed, leading to the conclusion that neither a global or local strategy is optimal for all control contexts.

4.2 Methods

4.2.1 Subjects

Three male rhesus macaque monkeys were used for this study. All procedures and animal care were conducted in compliance with the National Institutes of Health *Guide for the Care and Use of Laboratory Animals* and under the approval of UC Berkeley institutional review boards.

4.2.2 Cursor control task

Subjects were seated, head-fixed, in front of a computer display in which circular targets and a circular cursor appeared. The horizontal and vertical velocity of the cursor was controlled by either the position of a hand-operated joystick situated in front of the subject (joystick control), or the output of a BMI decoder (spike-BMI or LFP-BMI control). The subject was trained to initiate trials by positioning the cursor in the center of the workspace. Targets appeared one at a time randomly around an 8 cm radius circle and the subject was required to move the cursor to the target. If the cursor remained in the target for 200 ms, the trial was considered successful and a juice reward was delivered. Performance on individual trials was assessed by movement time, the time in seconds between the peripheral target's appearance and the completion of the hold in the target.

4.2.3 Velocity perturbation

Once subjects had mastered the cursor control task, a velocity perturbation was applied to the cursor movements by the addition of a constant vector to the output of the joystick or BMI decoder for the duration of the experimental session. The angle of this vector was chosen arbitrarily at the beginning of the session. The magnitude of the vector was calibrated for each subject individually such that it produced the largest possible movement-time differences among targets while still allowing the subject to successfully complete trials to all targets. The direction and magnitude of the added perturbation vector at any given time point were not dependent on the velocity command produced by the subject; they remained constant for all cursor position updates throughout the experimental session.

4.2.4 Surgery

Titanium headposts were surgically attached to each subject's skull surface along the posterior midline using 16 titanium bone screws. In a second surgery 6-12 months later, electrode arrays were implanted. The subject was anesthetized and the scalp and muscle incised along the midline to expose the skull. Craniotomies were performed over the pre-central motor cortical areas and arrays were placed bilaterally over M1 and PMd (256 total channels, Monkey G and Monkey S), or M1, PMd, and PMv (384 total channels, Monkey C). The precise craniotomy positioning was based on coordinates from an atlas and anatomical landmarks. Each array was slowly lowered into the cortex by stereotax to a depth of 2.5-3 mm, targeting layer V pyramidal neurons. After array placement, the craniotomies were filled with surgical wax and the entire site was covered by a rigid cap of dental acrylic, leaving only the array connectors exposed.

4.2.5 Electrophysiology recording

Chronic, high-density arrays of 128 (Monkeys G, S, and C) or 64 (Monkeys G and C) microwire Teflon-coated tungsten electrodes with 35µm diameter and 500µm spacing (Innovative Neurophysiology, Durham, NC) were used to record single- and multi-unit neural activity as well as local field potentials (LFP). Signals from M1 and PMv were used for this study. Voltage signals from the electrode channels were amplified and recorded using an OmniPlex data acquisition system (Plexon Inc, Dallas, TX). Spike sorting was performed online by the Omniplex system using principal component analysis and template matching. Local field potentials were low-pass filtered and a fast-fourier transform was performed to calculate power in several different frequency bands between 10 and 100 Hz.

4.2.6 BMI control and decoder adaptation

Under BMI control, a Kalman filter was used to map recorded neural activity to cursor velocity in real time. Two types of decoders were used in this study. Monkeys G and C performed the task with spike-BMI decoders, in which the signals used as the input to the BMI decoder are the firing rates of an ensemble of 10-200 individual neurons and multi-units (see Orsborn et al. (2012) for spike decoder implementation details). Monkeys C and S performed the task using LFP-BMI, in which the input to the decoder consisted of the spectral power across several local field potential frequencies (see Dangi et al. (2013) for LFP decoder implementation details).

At the beginning of each experimental session, subjects passively observed cursor movements on the screen for 3-5 minutes while brain activity was recorded. This recorded activity was used to generate the initial decoder calibration using the visual feedback decoder seeding method described in Orsborn et al. (2012). The subject was then required to perform the cursor control task for 5-10 minutes while a recursive maximum likelihood method of closed-loop decoder adaptation (CLDA) was iteratively performed in order to better match the decoder parameters to the subject's intended movements. Details about CLDA implementation can be found in Dangi et al. (2014). At the end of the CLDA block, the decoder was fixed for the remainder of the day's experimental sessions.

4.3 Results

4.3.1 Initial effect of velocity perturbation

Movement speed was generally consistent across targets after subjects were well trained on the cursor control task, but before the velocity perturbation was applied. For most subjects and control conditions, the velocity perturbation initially produced a global shift in the movement times, with improved (shorter) times for targets in the direction of the added vector and impaired (longer) times for targets in the opposite direction (see Figure 5.1A). Monkey G under joystick control exhibited slower times in all directions. Since the baseline movement times in this condition were shorter than those in the BMI conditions, this difference may be due to an ability to control the cursor's accuracy at very high movement speeds. However, the performance in this condition still showed a slight bias after the perturbation was applied, with longer movement times in some directions than others.

At the level of individual targets within sessions, all conditions exhibited a mix of movement time increases (positive differences) and movement time decreases (negative differences) between baseline and perturbed performance (Figure 5.1B).

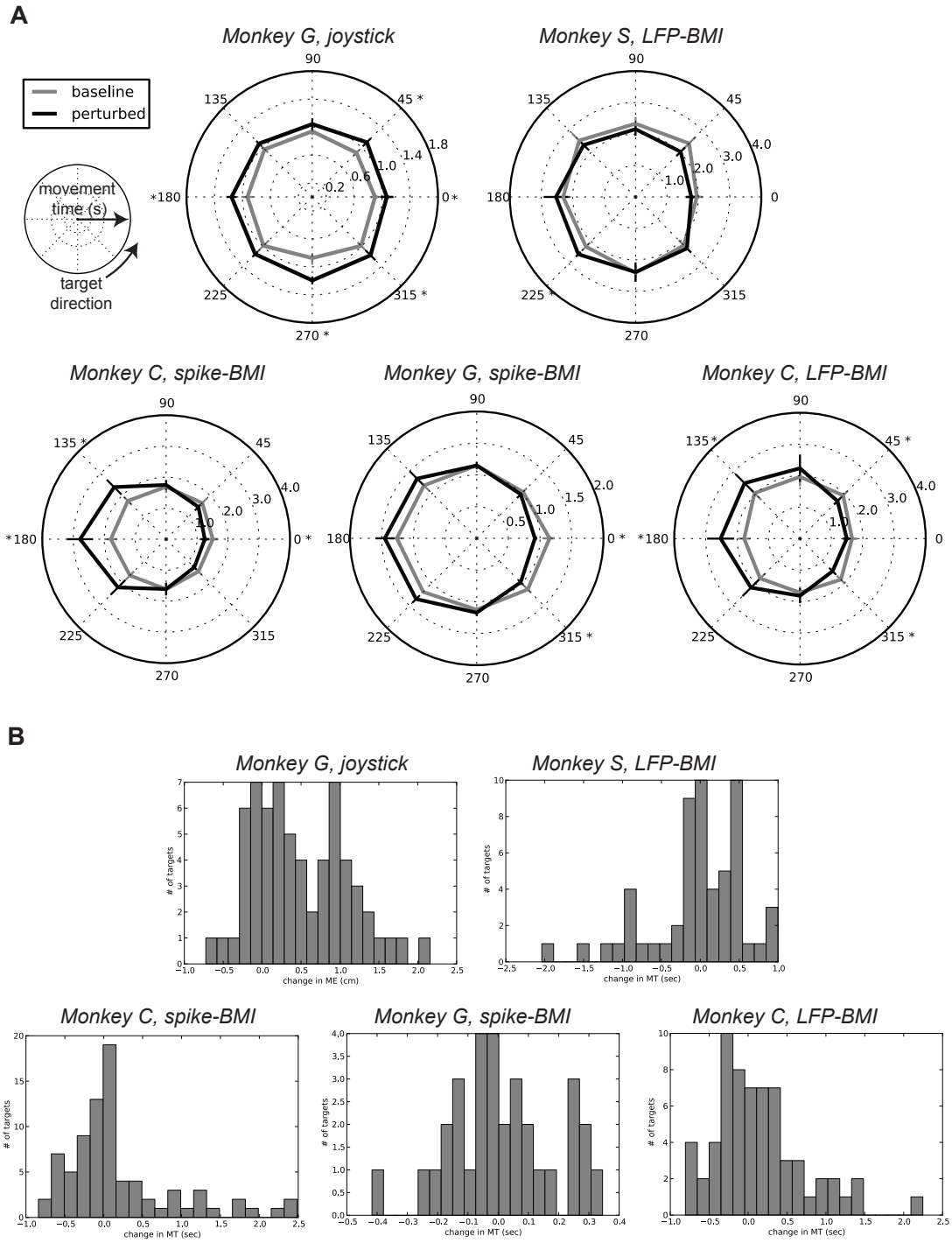

Figure 5.1: Effect of velocity perturbation on movement time. A) Initial effect of velocity perturbation on movement time for different subjects and control conditions. Each plot is averaged across all sessions for that condition with the target directions for each session's data rotated before averaging such that the perturbation direction is at 0 degrees. Typically, movement times decreased (faster movements) in the direction of the perturbation and increased (slower movements) in the opposite direction. B) Distribution of movement time changes (perturbed MT – baseline MT) across individual targets in individual sessions. In all conditions, targets demonstrating both speed increases and speed decreases were observed.

4.3.2 Adaptation to velocity perturbation

Adaptation strategies after practice with the perturbed system varied across subjects and conditions. On average, Monkey G with joystick control, Monkey S with LFP-BMI control, and Monkey C with spike-BMI control improved (decreased) movement times in the slowest directions while keeping those in other directions constant, consistent with a "local" adaptation strategy. In contrast, Monkey G with spike-BMI control displayed increased movement times such that the bias caused by the perturbation was exaggerated at the end of the adaptation session. Monkey C with LFP-BMI control exhibited no clear pattern when the data was averaged (Figure 5.2A).

At the level of individual targets on individual sessions, all subjects once again showed a mix of positive and negative movement time changes between the initial perturbed performance and the adapted performance (Figure 5.2B).

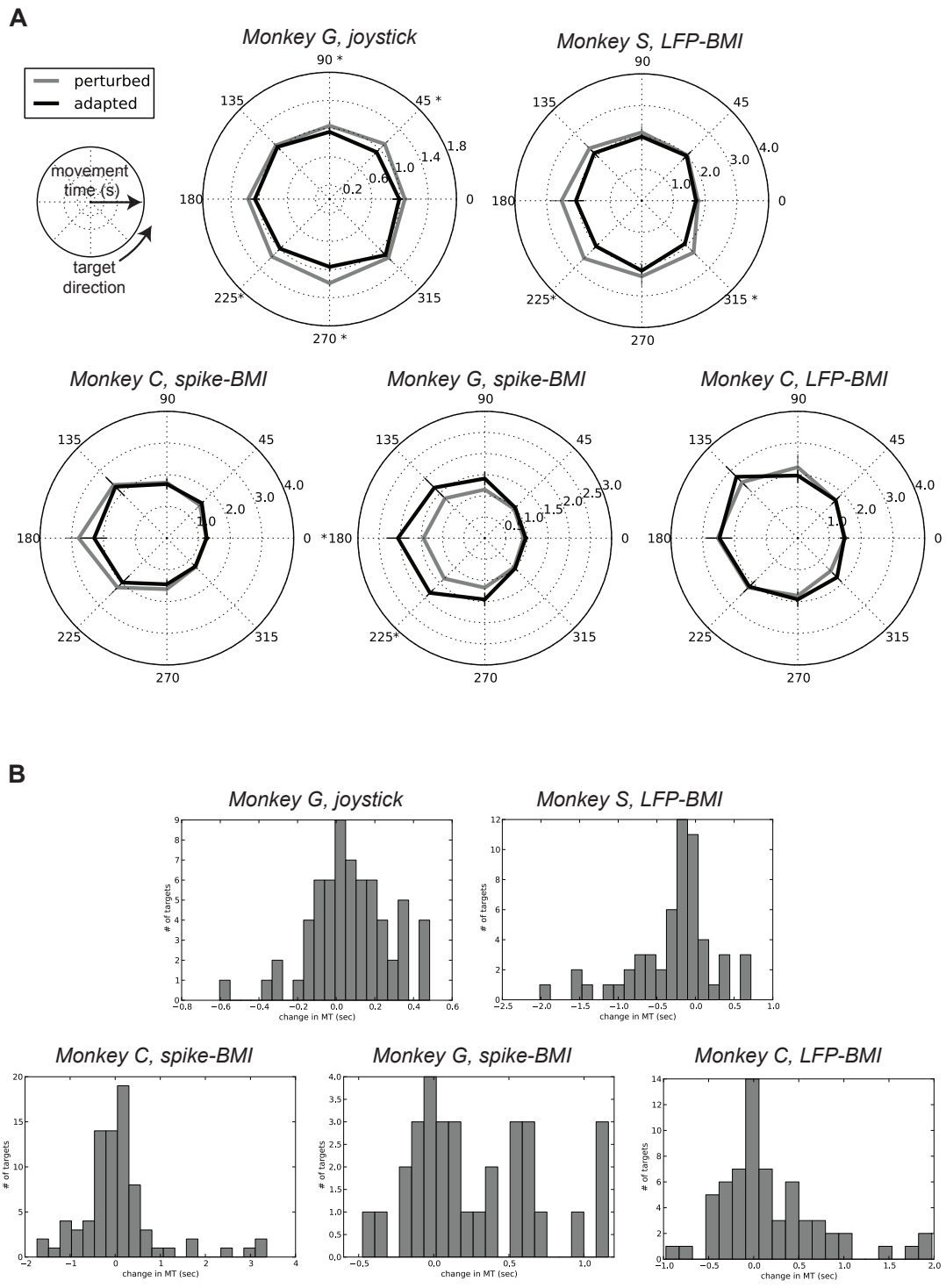

Figure 5.2. Adaptation to velocity perturbation. A) Average change in movement time for different targets with respect to perturbation direction. Each plot is averaged across all sessions for that condition, with the target directions for each session's data rotated before averaging such that the perturbation direction is at 0 degrees. A variety of different adaptation effects were observed across the 5 conditions. B) Distribution of movement time changes (adapted MT – perturbed MT) across individual targets in individual sessions. In all conditions, targets demonstrating both speed increases and speed decreases were observed.

To examine whether there was a consistent pattern in the degree to which the perturbation was counteracted or exaggerated across individual targets, the adaptation effect (difference between adapted and perturbed movement time) as a function of the perturbation effect (difference between perturbed and baseline movement time) was calculated for each condition (Figure 5.3). Once again, the varying strategies in different conditions were observed.

At one extreme, Monkey S with LFP-BMI control tended to counteract the perturbation regardless of the sign of the initial effect. Performance on targets for which movement times initially became longer because of the perturbation (points with positive x values in Figure 5.1) tended to improve, whereas performance worsened on targets for which movement times were initially shortened (points with negative x values). Furthermore, the magnitude of the adaptation effect was strongly predicted by the magnitude of the initial perturbation effect ($r = -0.57$). Monkey C's strategy with LFP-BMI control and Monkey G's strategy with joystick control appeared similar and also exhibited a negative correlation ($r = -0.39$ and -0.35, respectively), however it is difficult to determine with certainty whether the pattern would hold in the Monkey G/joystick dataset if it contained more examples of targets that experienced shortened movement times after the initial perturbation.

Monkey G's strategy with spike-BMI control also exhibited a clear pattern, with the perturbation effect magnitude highly correlated with the adaptation effect magnitude ($r = 0.71$). However, the direction of the effect was reversed from the examples discussed above so that targets that experienced increases in movement time due to the perturbation (positive x values) showed further increases in movement time after the adaptation period. Instead of counteracting the perturbation, this served to exaggerate it. Performance was negatively affected for the majority of targets, regardless of whether the initial perturbation increased or decreased their movement times.

Finally, for Monkey C's spike-BMI control data, no clear pattern emerged. Performance for targets that experienced decreases in movement time due to the perturbation (negative x values) tended to exhibit small amounts of adaptation in either direction but with no strong correlation (points clustered around $y = 0.0$). Targets with more extreme initial increases in movement time (positive x values) tended to exhibit correspondingly high magnitudes of adaptation; however, these examples were approximately evenly split between strong increases and decreases in movement time.

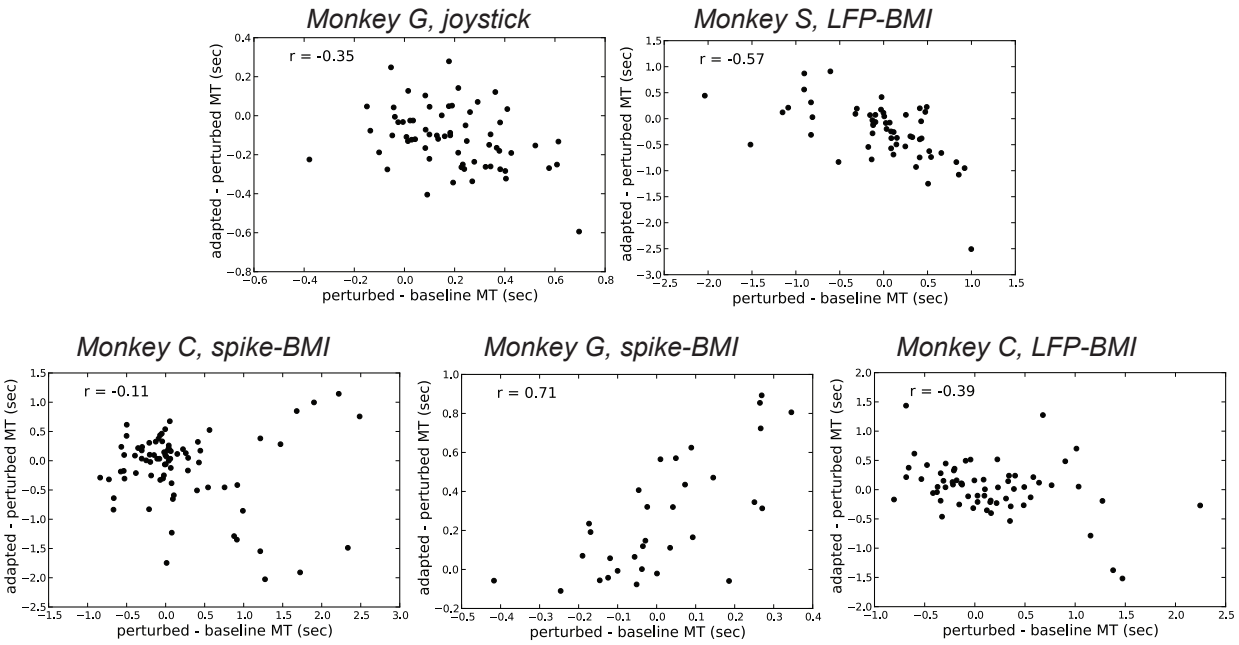

Figure 5.3: Predictability of adaptation effect based on perturbation effect across individual targets in individual sessions. The horizontal axes represent the magnitude and direction of the effect of the initial perturbation on individual targets and were calculated by subtracting the movement time during baseline trials from the movement time during early perturbed trials. Positive values indicate an increase in movement time (worse performance). Negative values indicate a decrease in movement time (improved performance). The vertical axes represent the same measure for the effect of the subject's adaptation after practice with the perturbation. Values were calculated by subtracting the movement time during early perturbed trials from the movement time during late perturbed trials. A variety of different patterns was observed across the 5 conditions.

4.4 Discussion

Depending on the subject and control paradigm, a variety of adaptation strategies were observed in this study, leading to the conclusion that neither a local or global strategy is the consistent solution to this type of perturbation. Monkey S's LFP-BMI control solution, and to a lesser degree, Monkey C's LFP-BMI control and Monkey G's joystick control solutions, support a global model of adaptation, with both the negative and positive effects of the initial perturbation across all the target directions being reduced back toward unperturbed baseline levels over time, even at the expense of performance on the targets to which movements were initially assisted by the perturbation (indicated by a negative correlation in Figure 5.3). However, the data from the remaining two conditions do not support this model. In fact, Monkey G's spike-BMI strategy displays a positive correlation in Figure 5.3 between initial effect of perturbation, and degree of adaptation after learning, indicating something of an exaggeration of the initial perturbation over time, (e.g. targets that are initially slowed down become slower, targets that are initially sped up become faster). One possible interpretation of this observation is that the subject adopted a strategy in which over time, more effort was directed toward trials requiring "easy" movement directions (directions that matched the perturbation direction), and less effort was directed toward "difficult" directions, perhaps allowing the maintenance of a certain acceptable overall

reward rate while reducing some type of mental or physical effort/cost. However, additional data would be needed to confirm such an interpretation.

An interpretation of the adaptation-related changes based on the changes due to the initial perturbation as in Figure 5.3 may be problematic because it assumes a perfectly unbiased baseline condition, whereas in reality small biases in movement times may exist across the target directions even before applying a perturbation. In these cases, the magnitude of the perturbation-related change is not necessarily equivalent to the overall amount of bias for a particular target compared to other targets, and examining the adaptation effect alone as in Figure 5.2 may be more meaningful.

When directly comparing the movement times before and after adaptation, both increases and decreases are apparent at an individual target level (Figure 5.2B), yet few increases are apparent when the data is averaged across sessions (with the exception Monkey G's spike-BMI data). In fact, 3 out of the 5 conditions displayed improved movement times for the slowest targets and little or no change in movement times for the fastest targets, supporting a local adaptation strategy in which changes in performance are selectively applied where improvements are required. This apparent discrepancy can be explained by the fact that the averaged data is oriented such that the perturbation directions align across sessions since these directions were chosen randomly each day. While there may be many examples of individual targets within individual sessions for which movement time increased by the end of the adaptation period, the increases are only reflected in the average if they occur in directions that are consistent with respect to the perturbation direction across days.

Overall, the range of different outcomes across the 3 subjects and 3 types of control conditions indicate that it is unlikely that an optimal strategy for adapting to a perturbation that has inconsistent effects across the workspace exists for all situations. Factors such as the overall difficulty of the task, type of feedback available, and control signal being used are likely to influence adaptation. Additionally, subject-specific preferences or strategies likely play a factor since different outcomes were observed across subjects even when the control condition was the same (e.g. Monkeys C and G with spike-BMI control or Monkeys S and C for LFP-BMI control).

The inconsistencies in the responses between subjects and between the natural motor control and BMI control versions of the task lead to the conclusion that a constant velocity perturbation is not an effective paradigm for studying motor control at a behavioral or neural level.

5 Control of redundant kinematic degrees of freedom in a closed-loop brain-machine interface

5.1 Background

The natural motor system displays impressive dexterity in controlling the many degrees of freedom (DOFs) of arm movements. The arm contains kinematic redundancy in the transformation from shoulder, elbow, and wrist angles to hand position in 3-D space as there are many possible joint postures to achieve a single endpoint position. However, the neural mechanisms that enable dexterous control of redundant plants remain an area of debate. It remains unclear whether motor cortical neurons represent kinematic or kinetic parameters, or whether they represent intrinsic (e.g., joint) coordinates or extrinsic (e.g., hand) coordinates (see (Scott, 2003) for an overview). Furthermore, the point in the sensorimotor loop when kinematic redundancy is resolved remains unclear. Early studies indicated that the brain attempts to resolve redundancy in the planning stages by minimizing a cost function such as kinematic jerk (Flash and Hogan, 1985), torque change (Uno et al., 1989), endpoint variance (Harris and Wolpert, 1998), etc. More recent studies have shown that variability in redundant dimensions may be greater than in "controlled" dimensions (Scholz and Schöner, 1999), possibly because movements in the redundant dimensions do not affect task performance and therefore controlling variability in those dimensions is unnecessary (Todorov and Jordan, 2002). In addition, the ability of the natural motor system to control redundant systems transfers to novel mappings. Human subjects can learn a novel redundant mapping between naturally generated high-dimensional finger movements and a 2-D cursor (Mosier et al., 2005; Liu and Scheidt, 2008; Liu et al., 2011). Neural control of redundant manipulators is an important open question in motor control.

Brain-machine interface (BMI) systems hold tremendous potential to restore motor function lost to neurological injury or disease. The focus of this work is on kinematically redundant BMIs, where the combination of task and plant under neural control allow for multiple, equally optimal, task solutions. Typical BMI paradigms are not kinematically redundant. An example is the 2-D cursor movement task where the two degrees of freedom (DOFs) defining cursor position are controlled by neural activity (Serruya et al., 2002; Taylor et al., 2002; Carmena et al., 2003; Musallam et al., 2004; Hochberg et al., 2006; Santhanam et al., 2006; Ganguly and Carmena, 2009; Suminski et al., 2010; Gilja et al., 2012). In the cursor paradigm, there is only one way for the prosthesis to achieve any specific cursor trajectory. In contrast, the paradigm we use in this work has two added DOFs that allow many different manipulator trajectories to produce the same endpoint trajectory.

Even when greater numbers of controllable DOFs exist in a BMI system, the corresponding tasks are generally not kinematically redundant. For example, several studies have demonstrated control of arm-like robots that are able to grasp objects in 3-D space, but these paradigms lacked kinematic redundancy since neural control was only allowed for the end effector, e.g., endpoint velocity and 1-D grip (Velliste et al., 2008; Hochberg et al., 2012). Any remaining mechanical DOFs remained under machine control and were not subject to neural input. Redundant kinematic solutions may have been possible in studies which supplemented 3-D velocity and 1-D grip with 3-D end effector orientation (Collinger et al., 2013) and multiple grasp dimensions

(Wodlinger et al., 2015), and were possible when functional electrical stimulation was used to drive different muscles with similar effects on hand grasp (Ethier et al., 2012). The presence of redundant solutions in those scenarios would depend on the objects being grasped, and redundant solutions were not the focus of those studies.

To our knowledge, no studies have explicitly investigated control of a BMI system that exhibits kinematic redundancy. In order to examine redundant control in BMI, we designed a virtual four-link kinematic chain that moved in a two-dimensional plane. With this system, any endpoint position could be achieved by an entire 2-D space of kinematic chain configurations. Two non-human primate subjects were trained to control the four joint velocities of the chain with neural activity in a closed-loop BMI system. Single- and multi-unit activity was decoded using a Kalman filter and the parameters of the Kalman filter were calibrated daily using closed-loop decoder adaptation (CLDA). The subjects were tasked with moving the endpoint of the redundant kinematic chain to instructed target locations. Hence, the subjects controlled more DOFs than were necessary to perform the task.

5.2 Methods

5.2.1 Surgery and Electrophysiology

Two adult male rhesus macaques (*Macaca mulatta*), Monkeys C and G, were used in this study. Monkey C was implanted with bilateral chronic Teflon-coated 128-channel tungsten microwire electrode arrays (35 micron diameter, 500 micron wire spacing; Innovative Neurophysiology, Durham, NC) for neural recording. Monkey G was implanted with a similar array in the left hemisphere but was implanted with two 64-channel arrays (same electrode diameter and spacing) in the right hemisphere. The arrays targeted the hand and arm representation areas of primary motor cortex and dorsal premotor cortex based on stereotactic coordinates. Single and multi-unit activity was recorded using a 256-channel Omniplex system and sorted online using PlexControl (Plexon, Inc., Dallas, TX). All procedures were conducted in compliance with the National Institute of Health Guide for Care and Use of Laboratory Animals and were approved by the University of California, Berkeley Institutional Animal Care and Use Committee.

5.2.2 Behavioral Tasks

The monkeys were trained on a virtual task in which they were required to move a cursor to an instructed target on a computer screen. After being trained to control the cursor with arm movements, the monkeys controlled the cursor with neural activity via a Kalman filter, which did not require overt arm movements. Once the monkeys had been familiarized with the brain-control cursor, they began controlling the joints of a four-link virtual kinematic chain with neural activity. Figure 5.1A illustrates the experimental setup. All tasks required moving the chain endpoint inside an instructed target (radius 1.3 cm for Monkey C, radius 1.5cm for Monkey G). They were given 7-15 seconds to complete each movement and needed to hold the endpoint inside the target for 200ms to receive a liquid reward. Failure to complete the movement in time or hold for sufficient time restarted the same trial without reward.

In the center-out task, illustrated in Figure 5.1B, the monkeys initiated trials at their own pace by holding the endpoint in the center for 200ms. Upon entering the center, the peripheral target appeared. After the center-hold period ended, the center disappeared, cuing the monkeys to

initiate movement to the instructed target. Instructed targets (16 for Monkey C, 8 for Monkey G) were uniformly spaced about an 8 cm radius circle.

After the monkeys were familiar with the kinematic chain center-out task, they performed the multi-configuration task, illustrated in Figure 5.1C. At the start of each trial, the endpoint appeared at the center of one of four uniformly spaced peripheral targets. For each starting position, we set $\theta_4 = -9$ degrees and θ_3 to one of {135, 157.5, 180, 202.5, 225} degrees for Monkey C or {135, 180, 225} degrees for Monkey G, in absolute coordinates. The remaining joint angles θ_1 and θ_2 are fixed if the endpoint is known (Burdick, 1989). This yielded a total of 20 and 12 possible starting postures for Monkeys C and G, respectively. In all trials, the monkeys were instructed to move the endpoint to a target at the center of the workspace. Unlike the center-out task, this task was not continuous since there was a large, automatic movement of the chain back to one of the preset configurations before each new trial.

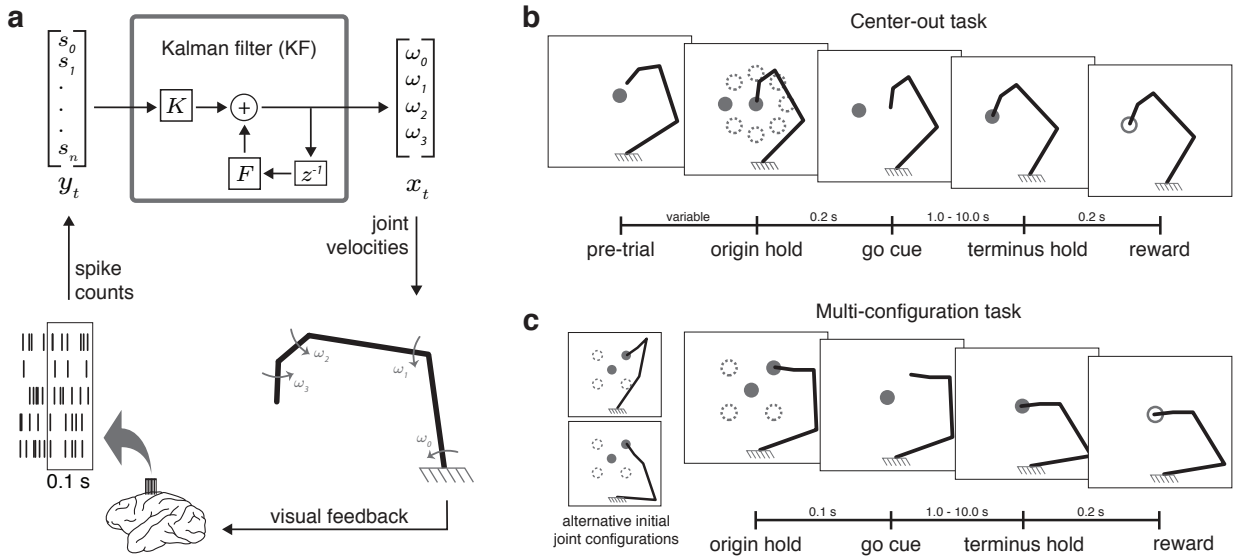

Figure 5.1: Experimental setup and task timelines. **A)** Closed-loop BMI control of the kinematic chain. Observations of single and multi-unit spike counts were used to decode the joint velocities of a four-link kinematic chain moving in a 2-D plane. **B)** Center-out task and timing. The subjects were required to move the chain's endpoint to the center to initiate trials and then move to a peripheral target. **C)** Multi-configuration task and timing. Subjects were required to move the chain's endpoint to the specified target, starting from one of 3 possible joint configurations per starting position for Monkey G, or 5 possible joint configurations per starting position for Monkey C.

In some sessions, we tested the effect of visual feedback of the chain configuration on multi-configuration task performance. On 50% of trials randomly chosen, the entire chain was hidden except for a cursor representing the endpoint. To determine whether the feedback reduction significantly impacted movement time, we used a randomization test. Since task performance varied by starting configuration, randomization was only performed within starting configuration.

For a small number of sessions that were analyzed separately, Monkey G performed a variant of the multi-configuration task with different starting configurations and instructed target locations. In each of these sessions, the starting configurations were selected such that the primary two principal components of the control signals (see *Control signal analysis and DOF manipulation* below) only allowed the endpoint to move in a single direction. That is, near these configurations, two DOFs in joint space only translated to one DOF in the endpoint space. In the robotics literature, such configurations are referred to as singularities. For each configuration, we placed the instructed target along the path of one of the remaining two principal components. This placed the target approximately perpendicular to the single path accessible to the primary principal components. An example is shown in Figure 5.4B. These combinations of starting configuration and instructed target were intended to elicit activity in the less prominent principal components.

5.2.3 Manipulator kinematics

Our subjects controlled the endpoint of a four-link virtual kinematic chain. The links of this chain, from proximal to distal, were 15cm, 15cm, 5cm and 5cm (selected arbitrarily). The four joint angles $\theta_1, \theta_2, \theta_3, \theta_4$ collectively specify the configuration of the chain. The endpoint position of the chain can be determined from the configuration by standard forward kinematics:

$$\begin{bmatrix} p_x \\ p_y \end{bmatrix} = f(\theta) = \begin{bmatrix} \sum_{l=1}^{N} l_i \cos\left(\sum_{k=1}^{i} \theta_k\right) \\ \sum_{l=1}^{N} l_i \sin\left(\sum_{k=1}^{i} \theta_k\right) \end{bmatrix},$$

in which $f(\cdot)$ is the forward kinematics function (Corke, 2011). For sufficiently small velocities ω and small time-scales Δ, the forward kinematics can be accurately linearized:

$$f(\theta_t + \Delta\omega_t) \approx f(\theta_t) + \Delta \frac{\partial}{\partial\theta} f(\theta)\Big|_{\theta=\theta_t} \cdot \omega_t = f(\theta_t) + \Delta J(\theta_t)\omega_t.$$

The manipulator Jacobian $J(\theta_t)$ is a 2x4 matrix mapping joint velocities to endpoint velocities. Thus it is possible to have joint velocities ω_{null} such that $J(\theta)\omega_{null} = 0$. These null velocities reconfigure the chain with little to no endpoint movement. In practice, such null velocities will induce a small endpoint movement due to linearization inaccuracies. For the maximum joint velocity we observed (0.6 rad/sec), this inaccuracy was less than 2 mm. In contrast, other velocities $\omega_{endpt} = J^{\dagger}(\theta)J(\theta)\omega_{endpt}$ in which $(.)^{\dagger}$ is the matrix pseudoinverse. These represent the smallest joint velocities (in the ℓ_2-norm sense) that produce a particular endpoint velocity. All joint velocities can be decomposed into an endpoint component and a null component: $\omega = \omega_{null} + \omega_{endpt}$.

For tasks in which the endpoint must move toward a specified target p^*, endpoint velocity can be further divided into a goal component, which moves the endpoint along the axis $g = \frac{p^* - f(\theta)}{||p^* - f(\theta)||}$,

and an error component, which moves the endpoint orthogonal to the goal axis. Thus we subdivide $\omega = \omega_{null} + \omega_{goal} + \omega_{error}$ in order to further analyze the endpoint component of joint velocities, using these equations:

$$\omega_{goal} = J^{\dagger}(\theta)g \cdot (J(\theta)\omega)^{T} g$$
$$\omega_{error} = \omega_{endpt} - \omega_{goal}.$$

5.2.4 BMI decoder architecture

In BMI systems, the decoder plays a central role in mapping the observed neural activity from the population of BMI neurons to kinematic control signals for the prosthesis. In this work, we utilize the Kalman filter (KF) as the decoder and calibrate it using closed-loop decoder adaptation (CLDA).

5.2.5 Kalman filter (KF)

Variants of the KF have been used in several online BMI experiments (Wu et al., 2006; Kim et al., 2008; Li et al., 2009; Gilja et al., 2012; Orsborn et al., 2012). When used to control our four-link virtual kinematic chain, $\tilde{x}_t$ represents the subject's intended joint angles ($\tilde{\theta}$) and joint velocities ($\tilde{\omega}$) at time *t*:

$$\tilde{x}_t = \begin{bmatrix} \tilde{\theta}_t^{(1)} & \cdots & \tilde{\theta}_t^{(4)} & \tilde{\omega}_t^{(1)} & \cdots & \tilde{\omega}_t^{(4)} & 1 \end{bmatrix}^T.$$

The KF estimates the hidden state $\tilde{x}_t$ when it follows the Gaussian process

$$x_{t+1} = Ax_t + \alpha BL\left(x_t - x_{eq}\right) + w_t; \; w_t \sim \mathcal{N}(0, W).$$

This model is a variant on the standard random walk model in which the walk is anchored around an equilibrium state x_{eq}. We hand-structured the state transition matrix *A* such that our model integrated joint velocities to update joint positions, structured the control input matrix *B* such that the inputs from the equilibrium state only affected the velocity states, and structured the state transition covariance *W* such that the process noise evolved independently for each joint:

$$A = \begin{bmatrix} I_4 & \Delta I_4 & 0 \\ 0 & 0.8 I_4 & 0 \\ 0 & 0 & 1 \end{bmatrix}, B = \begin{bmatrix} 0_4 \\ \Delta I_4 \\ 0 \end{bmatrix}, W = \begin{bmatrix} 0_{4\times 4} & 0 & 0 \\ 0 & 0.01 I_4 & 0 \\ 0 & 0 & 1 \end{bmatrix}. \quad (1)$$

Though we selected values 0.8 and 0.01 arbitrarily, they were effectively overwritten by the CLDA procedure described below (Gowda et al., 2014). *L* is an LQR-optimal infinite horizon feedback gain matrix (Shanechi and Carmena, 2013).

The observations y_t represent the spikes observed from a population of single and multi-units in the past 100 ms. The KF models $\tilde{x}_t$ and y_t as jointly Gaussian with the relationship

$$y_t = C\tilde{x}_t + q_t; \; q_t \sim \mathcal{N}(0, Q).$$

This model of neural firing assumes that spikes are linearly related to joint kinematics. In cursor BMI studies, modeling neural activity as relating to position variables was found to detrimentally impact performance (Kim et al, 2008; Gilja et al, 2012; Gowda et al 2014). Therefore, we only modeled the neural dependence on the joint velocity and did not model a relationship between neural firing and joint position. The KF algorithm recursively generates a new state estimate x_t using the previous estimate x_{t-1} and the most recent observation y_t:

$$\begin{aligned} x_t &= (I - K_t C)\left[A x_{t-1} + \alpha B L\left(x_{t-1} - x_{eq}\right)\right] + K_t y_t \\ &= (I - K_t C)(A + \alpha B L) x_{t-1} - (I - K_t C)\alpha B L x_{eq} + K_t y_t \end{aligned} \quad (2)$$

More KF details are presented in (Wu et al., 2004). For analysis purposes, it is convenient and sufficiently accurate to analyze the system as time-invariant, replacing K_t with the steady-state Kalman gain K as shown in Figure 1a (Gowda et al., 2014).

The value α controls how strongly movement toward the equilibrium affects the state of the prosthesis. In our previous work, we found that a similar tendency toward an equilibrium state arises spontaneously in decoders with position-based models of neural activity (Gowda et al., 2014). Similar strategies have been used to prevent "drift" due to inattention or disengagement during control of a 4-DOF robot (Velliste et al., 2008). For Monkey C, the equilibrium was unused ($\alpha = 0$), and we sometimes observed the kinematic chain entering into configurations in which he would lose motivation to perform the task, possibly because the chain configuration became difficult to manipulate. To prevent this issue for Monkey G, we used $\alpha = 0.025$ during the center-out task to keep the chain configuration from drifting too far from the equilibrium. Since the equilibrium posture's endpoint position was at the center of the workspace, the subject remained fully responsible for movements out toward the peripheral targets. This method was not applied to the multi-configuration task ($\alpha = 0$) since in that task the configuration of the chain was reset at each trial onset and the purpose of the attractor was to reduce the control burden during continuous control conditions.

5.2.6 KF parameter calibration using closed-loop decoder adaptation (CLDA)

Parameters were calibrated using closed-loop decoder adaptation (CLDA), an emerging paradigm for rapidly improving closed-loop BMI performance by re-estimating decoder parameters while the subject continues to operate the system (Taylor et al., 2002; Shpigelman et al., 2009; Gilja et al., 2012; Orsborn et al., 2012; Dangi et al., 2013). Parameter estimation procedures were adapted from (Orsborn et al., 2012; Dangi et al., 2014).

Initial parameters for C and Q were set by regressing against neural activity evoked when the subjects passively observed computer-generated movements of the kinematic chain. They were then iteratively re-estimated as the subject performed the task in closed loop. If the intended kinematics are known, then maximum-likelihood estimates of C and Q can be obtained by linear regression. While the intended kinematics cannot be obtained exactly, simple methods to infer intended kinematics based on the known goals of the task have been remarkably successful. For instance, the assumption that the subject always intends that the cursor velocity point toward the target has been used in several previous studies (Gilja et al., 2012; Orsborn et al., 2014).

The kinematic chain in this work has the added complication that the intended final joint angles are not fully specified by the intended endpoint location. To resolve this redundancy during CLDA, we constructed an arbitrary one-to-one mapping between target position p^* and intended configuration θ^* for each of the peripheral targets and the center target. CLDA was performed only on the center-out task. This mapping allows us to specify the goal state x^*, which we used to infer the intended kinematics by:

$$\tilde{x}_{t+1}^{est} = Ax_t + BL(x_t - x^*).$$

A, B and L are the same as in the KF state-space model. This intention estimation method is the multi-dimensional generalization of a feedback controller that slowly moves a cursor toward a target position (Gilja et al, 2012).

With the estimates of intended kinematics, we use the recursive maximum likelihood method to update C and Q (Dangi et al., 2014). This calibration procedure was repeated daily for both monkeys. After 5-10 minutes of decoder adaptation, the decoder parameters were fixed for the remainder of the experimental session.

5.2.7 Control signal analysis and DOF manipulation

In equation (2), the term $K_t y_t$ can be interpreted as a control signal to a linear system. The instantaneous contribution of the neural control is encapsulated entirely inside this term. Our control signals Ky_t are elements of a 4-D space. The control signal Ky_t has 9 elements because x_t has 9 elements. However, because we do not model neural dependence on joint positions and because the last element of x_t is constant, only the 4 velocity inputs are unique and the other 5 control inputs are linearly related to the velocity inputs. Hence we limit our analyses to $u_t = K_{[5:8,:]}y_t$, the 4-D joint-velocity control. Our tasks only require movement of the 2-D endpoint, resulting in two redundant DOFs. For our analysis, we decomposed the control signals into *goal, error,* and *null* components (see *Manipulator kinematics* above), symbolized as g_t, e_t, and n_t, respectively.

Additionally, we analyzed principal components (PCs) of u_t, which represent the uncorrelated joint co-activation patterns of maximal variance (Jolliffe, 2005). If p_i is the ith PC, then the component of a vector β along the ith PC is $\beta^{(i)} = p_i(p_i^T\beta)$. The scalar quantity $(p_i^T\beta)$is the activation of dimension p_i. This gives us a method to split u_t into 12 components:

$$u_t = g_t^{(1)} + \cdots + g_t^{(4)} + e_t^{(1)} + \cdots + e_t^{(4)} + n_t^{(1)} + \cdots + n_t^{(4)}.$$

We tested several hypotheses regarding the fraction of variance (FV) accounted for by various dimensions or combinations of these components. For example, to determine the fraction of each PC contributing to either endpoint or null movement, we calculated the FV for $g_t^{(i)} + e_t^{(i)}$ versus $n_t^{(i)}$. Or to test the relative contribution of each PC to g_t, we calculated the FV due to $g_t^{(1)}$, $g_t^{(2)}$, $g_t^{(3)}$, and $g_t^{(4)}$. The variance of each vector was calculated by adding the variances of each of the individual components (Jolliffe, 2005). Variance estimates were made using 1000 samples (100

sec) of data between the go cue and the terminus hold, and only observations from rewarded trials were considered (see Figure 1).

We also examined the similarity of DOF use across tasks. PCA is a data-dependent determinant of directions of maximal variance, and in addition to fluctuating across days due to changes in the decoder or neural population, may change across tasks. Thus when comparing DOF usage across tasks, we determined which DOFs were used during center-out control (PCs averaged across sessions and then re-orthogonalized using Gram-Schmidt orthogonalization) and then used these center-out DOFs to make meaningful comparisons of control strategies across task manipulations.

In some closed-loop experiments, we restricted u_t to 2 PCs. If $\bar{u}$ is the mean of u_t, then

$$u_t - \bar{u} = \sum_{i=1}^{4} p_i p_i^T (u_t - \bar{u}).$$

To allow N PCs, we substituted $\bar{u} + (\sum_{i=1}^{N} p_i p_i^T)(u_t - \bar{u})$ in place of Ky_t in equation (2).

5.3 Results

5.3.1 Subjects generated less stereotypic chain configurations as task performance improved

Both subjects successfully performed the center-out brain-control task with the 4-link kinematic chain. Figure 5.2A shows that movement time (the time elapsed between exiting the center and entering the target) decreased across days in both subjects (Monkey C: R^2=0.61, exponential fit; Monkey G: R^2=0.355, linear fit; p<0.02) over the course of 17-24 sessions. Figure 5.2B shows that average movement time was 0.76 s faster for Monkey C and 0.39 s faster for Monkey G in late (last 5) sessions compared to early (first 5) sessions. The distributions of movement times between early and late sessions were significantly different as well (Kruskal-Wallis test, $p<10^{-5}$).

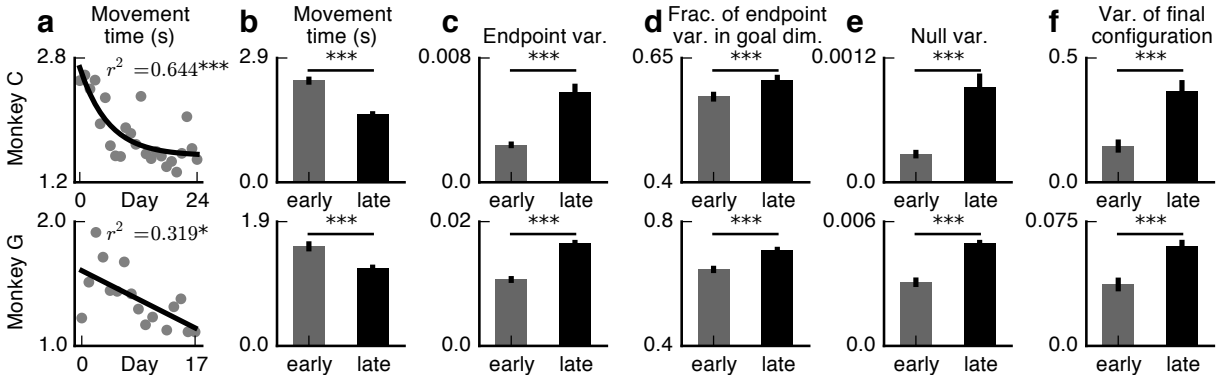

Figure 5.2: performance improvements across sessions correspond to shifts in endpoint and null velocity control signals. **A)** Both monkeys showed improved movement times across consecutive sessions on the center-out task. The performance improvements were significantly fit by an exponential curve for Monkey C (R^2=0.644, p<0.001) and a line for Monkey G (R^2=0.319, p<0.05). Early and late

sessions were defined for further analysis as the first five and last five sessions. **B)** Consistent with the curve fits from A, movement times significantly improved in late sessions (Kruskal-Wallis (KW) test, $p<0.001$). **C)** Endpoint velocity variance, corresponding to the range of control inputs which accelerated or decelerated the endpoint, increased from early to late sessions (KW test, $p<0.001$), consistent with faster movement times. **D)** Endpoint velocity was split into goal and error dimensions, indicating endpoint velocity control inputs on the axis toward the target or the axis orthogonal to the target, respectively. The fraction of endpoint velocity on the goal axis increased in late sessions (KW test, $p<0.001$), indirectly contributing to faster movement times by improving the instantaneous accuracy of endpoint control signals. **E)** Null velocity variance, corresponding to control inputs that altered the chain configuration without moving the endpoint, increased in late sessions (KW test, $p<0.001$). **F)** The increase in null variance likely caused an increase in the total variance of joint configurations at the end of the trial (KW test, $p<0.001$). Overall, in late sessions, the monkeys moved the endpoint of the chain to the target faster and in a larger range of final configurations. *:$p<0.05$, **:$p<0.01$, ***:$p<0.001$.

The joint-space control signals, u_t, were partitioned into endpoint and null components, and endpoint components were further subdivided into goal and error components (see Methods). Figure 5.2C shows that the variance of the endpoint component increased from early to late sessions for both monkeys (Kruskal-Wallis test, $p<0.001$). This increase suggests that in later sessions the monkeys utilized a broader range of control signals to accelerate or decelerate the endpoint. In parallel, we observed that in late sessions, a greater fraction of endpoint variability was related to control inputs along the goal axis than on the error axis (Figure 5.2D, Kruskal-Wallis test, $p<0.001$), and was likely responsible for an observed decrease in the endpoint path length across sessions for Monkey G ($r=-0.61$, $p<0.01$, linear fit). While Monkey C did not display a significant change in path length across sessions, he did demonstrate a decrease in the ratio of error variability to goal variability ($r=-0.81$, $p=0.008$, linear fit) as well as path length ($r=-0.54$, $p<0.001$) within-session. These improvements in performance are consistent with previous studies of co-adaptive BMI performance improvements (Taylor et al., 2002; Orsborn et al., 2014). Both monkeys were able to generate faster, more accurate endpoint control signals in late sessions, resulting in shorter movement times.

A more unique component of our study is the redundancy in the kinematic chain, which allows null movements to reposition the chain without moving the endpoint. Figure 5.2E shows that variability in the null dimension increased from early sessions to late sessions (Kruskal-Wallis test, $p<0.001$). On the behavioral level, we found that the configuration of the joints at the end of the trial became more variable across sessions. Figure 5.2F shows that the within-target, within-session configuration variance was significantly higher in late sessions than in early sessions (Kruskal-Wallis test, $p<0.00002$ for both monkeys). These increases in null motion and configuration variance are somewhat counter to previously published observations of natural motor remapping studies (Mosier et al., 2005), possibly because no physical movement is required for BMI control (see Discussion). The starting configuration of each trial, at the time of the go cue, was also more variable in later sessions than in early sessions (Kruskal-Wallis test, $p<0.0005$), and the starting configuration in a trial was highly predictive of the ending configuration. Averaging across targets and sessions, the starting configuration explained 94% of the variance in the ending configuration variance for Monkey C and 69% for Monkey G. This may indicate that the subjects attempted to optimize their solutions on a trial-by-trial basis depending on the configuration at the start of each trial rather than minimizing variability across trials.

Altogether, the changes in null and endpoint control components allowed the monkeys to move to the targets faster and achieve a wider range of final configurations without sacrificing endpoint performance.

5.3.2 Movement times were slower without joint configuration feedback

We analyzed the importance of direct visual feedback of the chain configuration state on task performance. The subjects performed the multi-configuration task with all links of the chain hidden on 50% of trials (randomly chosen), leaving only the chain's endpoint visible. The multi-configuration task was used to begin each trial with the chain at carefully controlled starting configurations and prevent the chain configuration at the end of one trial from impacting the strategy for the next trial. Since there were multiple possible joint configurations for each starting endpoint position, subjects could not determine the exact chain configuration from the starting endpoint position alone. We found that movement times were longer on average for these reduced-feedback trials. Across starting configurations, movement times when the links were hidden were on average 5.5% longer for Monkey C and 13.3% longer for Monkey G ($p<0.0001$, randomization test stratified by starting configuration; 3732 trials for Monkey C and 1763 trials for Monkey G). One configuration in particular required movement times that were 21.7% longer for Monkey C and 66.0% longer for Monkey G (Kruskal-Wallis test, $p<0.01$ corrected). This indicates that the control signal generated by the subjects was influenced by knowledge of the full configuration state of the redundant actuator and not exclusively the endpoint position.

To confirm that the observed feedback manipulation effect was specific to a plant in which the joint angles were not uniquely specified by the endpoint position, Monkey G performed a control experiment in which the four-link chain was replaced with a two-link chain. A two-link chain contains no kinematic redundancy, and the exact configuration of the joint angles can always be determined from the endpoint. Under these conditions, hiding the links had no effect on movement time ($p>0.35$, randomization test stratified by starting configuration; 4632 trials total). The importance of seeing the kinematic chain links was limited to the four-link chain that lacked a one-to-one mapping between endpoint position and joint configuration.

5.3.3 Redundant principal components of the neural control signal contributed to task performance

To extract the DOFs controlled during the continuous center-out task, we performed principal component analysis on the joint velocity control signals u_t. The resulting PCs represent four orthogonal patterns of relative joint co-activation that span the joint velocity space. Since the four-link chain possesses two excess DOFs to complete the center-out task, we aimed to determine which control dimensions were modulated by task goals by calculating the average activation of each of the PCs during trials to different targets. We hypothesized that PC activity due to noise would occur at a consistent level regardless of the intended endpoint movement direction, while activity due to goal-directed control would appear tuned to target direction. Figure 5.3A shows that activity along all four PCs showed clear direction-dependent tuning (cosine curve fit, $p<0.001$, averaged across sessions), with PCs 3 and 4 (the PCs with less FV) both most active during vertical endpoint movements. This suggests that despite the relatively

small fraction of variance explained by these PCs, they were tuned to the target direction and thus modulated by the goals of the task.

The PC tuning in Figure 5.3A was significant when averaged across sessions, indicating that DOFs were used in a consistent manner across center-out sessions. Since PCs are defined by a particular set of joint movement observations and therefore may vary depending on the decoder, the neural ensemble, and the requirements of a given task, we also computed more general DOFs based on average PCs across multiple sessions of the center-out task (see Methods). Figure 5.3B shows that the first two DOFs had larger FV than the last two DOFs. Thus we refer to the first two DOFs as primary DOFs (pDOFs) and last two as secondary DOFs (sDOFs). To determine how each DOF contributes to movement of the endpoint, we partitioned each DOF into null and endpoint components. Figure 5.3C shows that the pDOFs were more than four times more active in the endpoint dimension than in the null dimension for both monkeys (Kruskal-Wallis test, $p<10^{-7}$), while the reverse was true for the sDOFs (Kruskal-Wallis test, $p<10^{-7}$). From this, we concluded that the pDOFs were the main drivers of endpoint movement during center-out control.

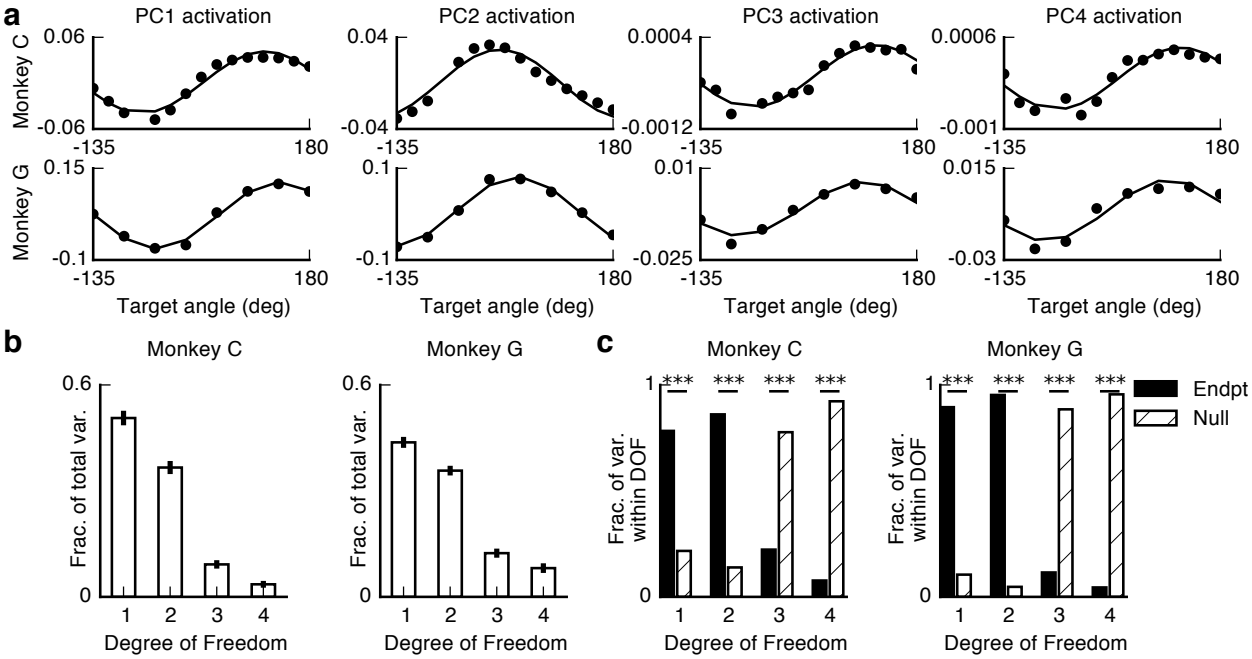

Figure 5.3: principal components (PCs) and degrees of freedom (DOFs) during center-out control. **A)** For the center-out task, we calculated PCs of the joint velocity control space (see Methods) and plotted the average tuning of these PCs to target direction across sessions. All PCs were significantly fit by a cosine tuning function ($p<0.001$). **B)** Fraction of variance (FV) along each DOF, averaged across sessions. Center-out DOFs were constructed by averaging the center-out PCs from individual sessions (see Methods). Center-out control was dominated by the use of the "primary" DOFs 1 and 2 (pDOFs), while the "secondary" DOFs 3 and 4 (sDOFs) accounted for a much smaller FV. **C)** Within each DOF, we calculated the average FV by either endpoint or null movements. Activity in the pDOFs was primarily endpoint movement while activity in the sDOFs was primarily null movement.

We asked whether the seemingly minor contribution of the sDOFs to center-out control reflected a global, task-independent control strategy, or whether there were regions of configuration space not traversed during the center-out task where the sDOFs might play a more prominent role. We examined the usage of these same sDOFs during the multi-configuration task, in which a more varied range of joint configurations occurred than in the center-out task. Figure 5.4A illustrates sDOF use by target location (center-out task) or starting configuration (multi-configuration task). For many starting configurations of the multi-configuration task, the fraction of endpoint variance due to sDOFs was higher observed during the center-out task. To further explore this effect, we had Monkey G perform a modification of the multi-configuration task specifically designed to encourage movements using secondary PCs and to penalize activity in the primary PCs (see Methods; an example is shown in Figure 5.4B). When controlling from these configurations, fraction of endpoint variance due to the sDOFs increased significantly (Figure 5.4A, "Singular Primary PCs") relative to both the standard multi-configuration and the center-out tasks. The sDOFs contributed 33% of endpoint movements from these configurations despite only contributing 13% during center-out control. Furthermore, the fraction of goal variance due to the sDOFs was on average 75% from these configurations. Not only were the sDOFs responsible for a large portion of endpoint movement from these particular configurations, they were primarily responsible for movements toward the goal.

We observed that faster trials in the multi-configuration task had a greater FV due to sDOFs. In all trials for this analysis, the entire chain was visible. For each starting configuration, we split trials into two groups based on whether they were faster or slower than the median movement time for that starting configuration. Figure 5.4C shows that the fast trials (aggregated over all starting configurations) tended to utilize more sDOF activity than the slow trials (Kruskal-Wallis test, $p<0.001$). This same result held within-configuration for 10 of 20 configurations for Monkey C and all 12 configurations for Monkey G (Kruskal-Wallis test, $p<0.01$ Holm-Bonferroni corrected). This relationship indicates that sDOFs enhanced task performance.

We performed a separate supplemental control experiment to confirm non-trivial contribution of the sDOFs during center-out control. Monkey G performed the center-out task with a decoder that was manipulated to only allow movement along the first two PCs, and the performance of this was compared to performance with the full four PCs (1189 trials in each condition, four PC data was collected on the same sessions as two PC data and did not overlap with any data in Figure 5.2). Average movement times were 11% worse in the 2-PC condition and increased significantly from 1.28 s to 1.42 s (Kruskal-Wallis test, $p=0.002$). The performance gap was most significant when moving toward targets at -90 (0.83s (49.1%) difference, $p<0.001$ corrected), -45 (0.32s (21.1%) difference, $p<0.001$ corrected), and 180 degrees (0.15s (13.0%) difference, $p<0.05$ corrected). These directions also exhibited corresponding large fractions of endpoint variance due to the sDOFs (Figure 5.3A).

Altogether, these results indicate that despite the 2-D nature of the task, the subjects' control strategies utilized the redundant sDOFs in addition to the pDOFs. The relative usage of sDOFs depended on the specific task requirements, and in fact, for some parts of configuration space, the sDOFs defined by the center-out task were more important than the pDOFs.

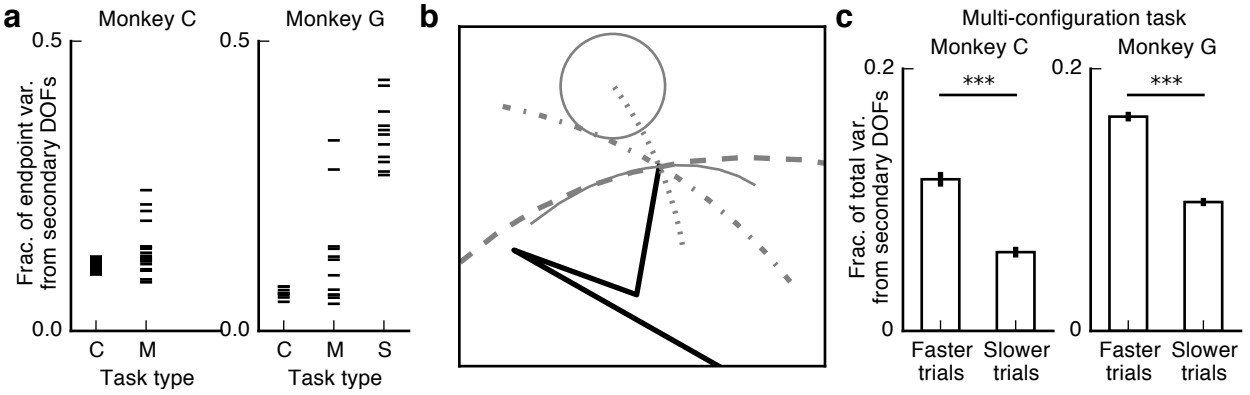

Figure 5.4: contribution of secondary degrees of freedom (sDOFs) to BMI control and performance. **A)** Comparison of fraction of variance due to sDOFs across different tasks (C: center-out, M: multi-configuration, S: Singular Primary PCs). Some starting configurations in the multi-configuration task showed a greater usage of sDOFs than in the center-out task, while even greater sDOF utilization was observed in a modified version of the multi-configuration task in which configurations and target locations were arranged to penalize primary DOF (pDOF) use and encourage sDOF use (Singular Primary PCs, Monkey G only). This demonstrated that the reliance on pDOFs observed during the center-out task was due the specific task requirements and not a global inability to modulate the sDOFs. **B)** An example configuration for the modified multi-configuration task to encourage sDOF use. Velocity control signals from PCs 1 and 2 generate endpoint velocities that are roughly parallel to each other and orthogonal to the direction of the target, while control signals along PCs 3 and 4 generate endpoint velocities toward the target. **C)** On the multi-configuration task, trials with faster than median movement times tended to have a larger fraction of total variance from sDOFs than trials with slower than median movement times.

5.4 Discussion

The restoration of upper limb function is one of the most common goals of BMI research. To fully match the functionality of the natural arm, a BMI system must provide the neural circuitry a mechanism for generating specific joint postures in addition to hand movements, an ability that is essential for certain types of movements such as reaching around obstacles. Providing the user with direct control at the joint or even muscle level is one possible way to incorporate this functionality. Studies involving robotic BMI control have typically only allowed direct neural control of the end effector (Carmena et al., 2003; Velliste et al., 2008; Hochberg et al., 2012; Collinger et al., 2013), with the generation of a corresponding configuration-space trajectory (e.g., joint positions) left to robotic path planning algorithms. Systems that instead seek to reanimate the natural limb through functional electrical stimulation of intact muscles have the potential to allow control of redundant aspects of the limb state, but relatively few examples of this type of control have been published. In a recent study in which brain activity directly controlled functional electrical stimulation (FES) of 3-5 hand and arm muscles to perform a grasping task (Ethier et al., 2012), the stimulated muscles likely formed a redundant mapping to the subjects' grasp. The FES paradigm demonstrates the clinical value of understanding neural control of redundant actuators.

It is important to note that the neural redundancy present in many BMIs is distinct from kinematic redundancy. Most BMIs contain neural redundancy in that there are typically many more neurons directly involved in closed-loop control than there are controllable DOFs in the

plant. However, there is an important distinction between kinematic redundancy in the manipulable DOFs of the plant and redundancy in the neural control signal: the user receives direct sensory feedback about the redundant plant state, but feedback about the state of individual redundant neural inputs can only be gained indirectly through observation of their combined effect on the plant. Because BMIs are closed-loop control systems, this difference in feedback conditions may result in the two types of redundancy exerting different effects on subjects' control. The impact of neural redundancy on BMI performance remains an open question and deserves further study.

A series of experiments investigated abstract motor learning of kinematically redundant maps (Mosier et al., 2005; Liu et al., 2011; Mussa-Ivaldi et al., 2011; Ranganathan et al., 2013, 2014). Subjects learned novel mappings from high-dimensional 19-DOF hand position to 2-D cursor position in order to perform cursor movement tasks. This paradigm differed from ours in that it remapped natural hand kinematics rather than utilizing direct cortical control of the redundant parameters. Subjects performing the hand-to-cursor control tasks reduced variability of the cursor position space by producing straighter trajectories, and reduced variability in the null position space by acquiring the target in more consistent configurations (Mosier et al., 2005). However, this null variability was not eliminated completely, and with continuous visual feedback subjects used remaining null movements to reduce energetic control costs (Ranganathan et al., 2013). In our data, we observed an *increase* in null variability in the velocity space as well as an increase in variability of the chain configuration at the end of the trial. This difference in strategy may be due to different cost functions between the two paradigms. The cost of null movement in our study is the metabolic cost of spiking activity to produce null movement, but it is unclear how to relate that cost to the cost of physical movement as in the hand remapping studies, or how to determine the cost of reshaping the network dynamics to suppress the null activity. It may have been difficult or impossible to generate neural activity to increase task-relevant speed without also generating larger null velocity components. In our paradigm, the more efficient strategy was apparently to increase null variability, consistent with a minimum intervention strategy in which the subjects learned to ignore or exploit motion in the null space rather than try to correct it (Todorov and Jordan, 2002).

Both subjects in our study engaged the redundant plant DOFs in small but non-trivial amounts. The coarse elements of control were dominated by the first two DOFs, but the third and fourth DOFs still influenced finer aspects of control. This control structure is similar to redundant DOFs that are engaged in natural motor control. For example, in hand grasping postures, though most of the postural variance can be explained by the first 2 PCs (>80%), the higher order PCs still contain information about the object being grasped (Santello et al., 1998).

While our subjects demonstrated that control of the redundant elements of the BMI plant can be achieved, it remains unclear whether permitting control of redundant DOFs would be advantageous in a clinical BMI system. Proprioception plays an important role in natural movement (Pearson, 1993) and a few studies have shown improved BMI performance when some form of proprioceptive feedback was provided (Suminski et al., 2010; Gomez-Rodriguez et al., 2011). Despite this, most BMI implementations are limited to visual feedback of a disembodied actuator. Under these impoverished sensory feedback conditions, it may be that increasing the number of controllable DOFs significantly increases the cortical control burden.

Extensive practice at controlling such a BMI system could potentially alleviate this issue to some degree, as many studies have demonstrated the brain's remarkable plasticity in learning both novel motor (e.g., Karni et al., 1995; Nudo et al., 1996; Kleim et al., 1998, 2004; Li et al., 2001) and BMI skills (Fetz, 1969; Jarosiewicz et al., 2008; Moritz et al., 2008; Ganguly and Carmena, 2009, 2010; Koralek et al., 2012). However, clinical studies have shown that ease of use and training are important factors in patients' decisions to accept and use prosthetics (Atkins et al., 1996; Biddiss and Chau, 2007). Thus in practice there will be a tradeoff between the complexity of learning to operate the system and the potential advantages of controlling more DOFs. Evaluating this tradeoff may be important to future clinical deployment of BMIs.

While our CLDA methodology was sufficient for subjects to achieve control of the plant in this study, it may be suboptimal for a redundant system since the presence of kinematic redundancy complicates the process of estimating intended movements for decoder calibration. Related calibration issues were raised by Collinger and colleagues (Wodlinger et al., 2015). Inferring the exact intended trajectory is never possible with any CLDA method, even when the optimal final state for a movement can be determined exactly. Our system poses the additional difficulty that for an endpoint movement task, the redundancy makes it such that any element of a 2-D state subspace is equally optimal. Our CLDA method makes strict assumptions about the goal pose of the kinematic chain. This method could be adapted to the plant of a clinical BMI system if a similar set of instructed configurations can be specified (e.g., useful limb postures for activities of daily living). Alternative CLDA methods based on reinforcement learning (e.g., Mahmoudi and Sanchez, 2011) or LMS-like methods to minimize endpoint error (Danziger et al., 2009) may also achieve high performance without explicitly assuming the subject is trying to attain a particular chain configuration. Further experiments are necessary to test these and other methods for redundant systems. However, no matter how good the CLDA method may be, the lack of sensory feedback compared to natural motor control is likely to remain a problem.

The BMI paradigm introduced in this study provides a potential framework for investigating elements of motor learning. For example, the concept of muscle synergies involves a mapping from a redundant parameter space to one with fewer DOFs (see (Tresch and Jarc, 2009) for a review). A redundant BMI system in which muscle activations are decoded could provide a useful test bed for synergy theories by enabling researchers to easily specify or disable synergies at will and observe the resultant effects on control, learning, and adaptation. Such "virtual lesions" have been proposed to study myoelectric control (e.g., Berger et al., 2013). One strong confound to these studies in natural motor control may be force of habit in muscle coordination (de Rugy et al., 2012). In an environment with novel geometry, such as a non-biomimetic plant, this problem may be mitigated. Though other novel environments can test control hypotheses (Mosier et al., 2005), BMI systems may also provide a valuable insight into how cortical structures may be involved in learning novel redundant systems and compensating for loss in redundancy.

6 Design of closed-loop BMI systems

The design and performance optimization of BMI systems is extremely important for advancing the capabilities of BMI as a clinically viable technology and maximizing the usability, robustness, and flexibility of neuroprosthetic control. The brain's natural plasticity is a critical element in closed-loop BMI systems, and BMI architectures must take into account (and ideally take advantage of) learning, adaptation, and error correction on the part of users during closed-loop control. The studies outlined in this chapter explore various elements of the interaction between the decoder and the brain during BMI control and may be used to inform the design of applied BMI systems. The studies summarized in this chapter represent the author's efforts to contribute more broadly to the advancement of the field of brain-machine interface research through collaboration on projects outside of the primary dissertation research areas described in previous chapters. For complete descriptions of the work described in sections 6.1, 6.2, and 6.3, refer to the accounts in Orsborn et al., (2014), Dangi et al., (2014), and Shanechi et al., (2015), respectively.

6.1 Closed-loop decoder adaptation shapes neural plasticity for skillful neuroprosthetic control

Evidence from many studies has shown that there are distinct differences in cortical activation patterns during natural movement vs. BMI control . One likely explanation for these differences is the brain's natural inclination to adapt its response based on sensory feedback about the state of the system it controls (Fetz, 2007; Ganguly and Carmena, 2009; Green and Kalaska, 2011; Koralek et al., 2012; Wander et al., 2013). When exercised in a BMI context, this neural plasticity appears to drive the development of distinct functional cortical maps between patterns of neuronal firing and actuator movements. These maps are strengthened with practice, and once learned are stable, rapidly recallable, and resistant to interference (Ganguly and Carmena, 2009).

Capitalizing on these natural learning properties could be advantageous for BMI by reducing the reliance on complex machine learning algorithms and increasing generalizability to new control contexts. However, a large degree of stability in the recorded brain signals used for control is required to enable this plasticity to occur. Obtaining this type of stability over days or months is difficult due to electrical noise in the signals, micro-movement of implanted electrode wires within the brain tissue, and signal degradation over time because of imperfect hardware biocompatibility.

For this reason, a number of groups have relied on methods of closed-loop decoder adaptation (CLDA) to improve performance in BMI systems as an alternative to natural plasticity (Taylor et al., 2002; Jarosiewicz et al., 2008; Li et al., 2011; Gilja et al., 2012; Orsborn et al., 2012; Dangi et al., 2013). These methods use short, frequent (usually daily) calibration sessions in which the parameters of the decoder are iteratively adjusted in real time as a subject performs a simple BMI task according to a set of assumptions about the subject's true movement intentions. In this way, discrepancies between the decoder and the subject's underlying neural representation of the movements may be reduced and performance improved without the subject being required to alter their strategy.

Little is known about the details of the ways in which brain and decoder adaptation interact with each other in a BMI system. Specifically, a large amount of CLDA may preclude neural plasticity by making the decoder a "moving target" for the brain to learn. This study tested the degree to which the type of subject-driven learning observed in fixed-decoder, non-adaptive BMI paradigms occurs in the presence of decoder adaptation, referred to as co-adaptation.

A BMI paradigm was developed in which CLDA was used intermittently over a period of 1-2 weeks to supplement natural plasticity during BMI control for two non-human primate subjects. Performance on a center-out BMI cursor task improved over the training period. Cortical maps became more consistent across days as learning progressed, indicating the formation of a stable neural representation of the decoder despite the periodic parameter changes due to CLDA. Throughout the learning process, the degree of map stability and the amount of change in modulation depth and preferred direction of observed neurons were correlated with the amount of performance improvement. Additionally, performance on the BMI task was resistant to interference by intermittent sessions of a task that required simultaneous arm and BMI movements, and neural tuning became more similar between the two tasks late in learning.

These results indicate that CLDA does not preclude the formation of the stable neural maps associated with pure learning BMI paradigms, and that the degree and type of neural adaptation that occurs over time is related to the amount of performance improvement. Further work is needed to determine whether co-adaptation paradigms can outperform purely plasticity-driven or machine-learning driven paradigms. A full report can be found in (Orsborn et al., 2014).

6.2 Continuous closed-loop decoder adaptation with a recursive maximum likelihood algorithm allows for rapid performance acquisition in brain-machine interfaces

Typically, BMI decoders are created by fitting filter parameters with neural training data collected while a subject made (Serruya et al., 2002; Taylor et al., 2002; Carmena et al., 2003; Musallam et al., 2004; Santhanam et al., 2006), observed (Orsborn et al., 2012, 2014), or imagined (Hochberg et al., 2006; Wahnoun et al., 2006; Kim et al., 2008; Velliste et al., 2008; Suminski et al., 2010) movements. Control performance is then improved online either through brain plasticity, decoder adaptation, or some combination of the two as the subject practices controlling the system.

Closed-loop decoder adaptation (CLDA) refers to the practice of iteratively adjusting the decoder parameters online during BMI control in order to improve the match between the decoded output and the underlying movement intentions. Various CLDA paradigms have been utilized in a number of published BMI demonstrations (Taylor et al., 2002; Gage et al., 2005; Heliot et al., 2010; Li et al., 2011; Gilja et al., 2012; Orsborn et al., 2012). Minimizing the time required for this calibration procedure is desirable in BMI applications in order to minimize subject frustration stemming from poor initial control, as well as reduce the time required to initialize the BMI system. One potential way to accomplish this is to increase the frequency of filter parameter updates during CLDA so that performance improvements can be experienced by the subject more immediately.

While such an approach is technically possible for adaptation algorithms based on stochastic gradient descent, the limited size of the resulting data batches (e.g., a single data point) used for each update can lead to inaccurate parameter updates that fail to converge (Orsborn et al., 2011). In this study, a recursive maximum likelihood (RML) algorithm was developed and tested for a BMI control task in three non-human primate subjects. The RML algorithm updated the parameters of the Kalman filter (decoder) continuously using all available prior data at each time step, weighted by recency.

Compared to SmoothBatch, a previously published batch-based CLDA algorithm (Orsborn et al., 2011), RML produced significantly better BMI performance after 5 minutes of adaptation time. After 10 or more minutes of adaptation time, RML performance was typically better than SmoothBatch performance, but the differences were not significant. Furthermore, sessions in which subjects failed to perform any successful trials were more common with SmoothBatch than with RML, indicating that RML successfully reduced subject frustration leading to early loss of motivation.

These results indicate that the RML CLDA algorithm successfully addresses problems of over-fitting and computational expense associated with other continuous adaptation methods to produce performance that is equal to or better than a commonly used batch-based algorithm. Additionally, RML outperformed SmoothBatch at short adaptation times, making it a potentially useful tool in BMI applications in which performance must be maximized in the shortest time possible. A full report can be found in (Dangi et al., 2014).

6.3 Rapid control and feedback rates in the sensorimotor pathway enhance neuroprosthetic control

Closed-loop BMI systems contain both a feedforward control pathway and a sensory feedback pathway for information. Little is known about the relationship between the temporal resolution of these pathways and neuroprosthetic control. Natural motor studies have shown that manipulating feedback rates can affect motor control strategies (Slifkin et al., 2000; Sosnoff and Newell, 2005), however direct manipulations of the control rate are not feasible in the natural motor system because they would involve interventions in the pathway between the brain and muscles. In a BMI system however, both feedback rate and control rate may be manipulated by the experimenter since the control signal from the brain is mapped through an artificial decoding algorithm.

In this study, the control and feedback rates in a closed-loop BMI system were independently manipulated, and the resulting performance effects were observed in a BMI cursor control task performed by two non-human primate subjects. These manipulations were performed with a novel point process filter (PPF) decoder for which neural firing model assumptions are valid even at very fast (5-16 ms) timescales. The control rate could be adjusted by changing the frequency with which the decoded movement command was sent from the decoder to the task, and the feedback rate could be adjusted by changing the frequency with which the cursor position was updated on the computer screen.

Both higher control rates and higher feedback rates were found to contribute to significantly improved performance on the BMI task. Additionally, the PPF decoder itself was demonstrated

to yield superior performance when compared to a state-of-the-art Kalman filter (KF) decoder with the same control and feedback rates.

7 Concluding remarks

7.1 Summary of contributions

In Chapter 2, we introduced a newly designed integrated, modular software suite for collecting experimental data and running real time experiments. The BMI3D software package was created to address two common needs in real-time control laboratories: to synchronize and stream data from multiple hardware sources and to create a powerful, integrated framework for the generation of experimental tasks and stimuli. Additionally, BMI3D's built-in tools for automatically storing and accessing large amounts of data have increased efficiency in data analysis and reduced issues of data loss or inaccuracy due to user error. Since its inception, BMI3D has been implemented in various forms in five experimental rigs. A number of researchers have collaborated on adding and refining features, and the package will be released under an open source license in the future for other members of the research community to utilize and improve upon.

In Chapter 3 we laid the groundwork for integrating the ventral pre-motor cortical area into a BMI system, either as a source of control signal or as a focus of observation for neuroscience questions concerning motor learning and sensory representation. We found that bimodal sensory neurons could be observed using a chronically implanted array, and confirmed previous findings demonstrating their sensory and motor response properties.

In Chapter 4 we explored adaptation strategies under a novel type of feedback perturbation. First, we established that such a perturbation had an inconsistent effect on performance during a cursor movement task; that is, it impaired performance for some movements but improved performance for others. We then tested several hypotheses about how the brain might adapt to a perturbation with these qualities. Ultimately we established that adaptation strategy depended heavily on the specific control context, task, and subject and that no consistent adaptation model was supported by our data.

In Chapter 5 we investigated the details of subjects' control strategy in a BMI system containing kinematic redundancy in the actuator. We established a two-dimensional redundant paradigm that enabled testing of questions regarding high-dimensional control on a flat display. We showed evidence that subjects are capable of actively controlling "extra" degrees of freedom when they are available. We also compared the high-dimensional control strategies observed in our BMI task with those previously observed in high-dimensional natural motor control tasks and discussed the degree to which our data supports established motor control theories regarding redundancy.

In Chapter 6 we explored issues related to decoding algorithm design, decoder adaptation methods, and the interaction between decoder adaptation and functional neuroplasticity in during BMI control.

7.2 Open questions

7.2.1 Ventral pre-motor cortex (PMv) as a control area for BMI

PMv's involvement in motor planning and arm movements, as well as its status as a sensorimotor association area make it a potential candidate for a BMI control area, but no studies explicitly comparing the quality of control signals between PMv and other motor areas such as primary motor cortex (M1) and dorsal pre-motor cortex (PMd) have been carried out. Because of PMv's unique motor-sensory association properties and its implication in reach-and-grasp movement activities, signals from this area may potentially be useful for improving BMI control either as an alternative to, or in addition to, those from traditionally targeted motor areas.

7.2.2 Incorporation of artificial actuators into PMv sensorimotor representation

Neurons in PMv are known to exhibit responses to visual and tactile sensory stimuli around the body, and their receptive field characteristics have been shown to be sensitive to recent experience in controlling actuator attached to the body. An open question is whether or not PMv neurons are part of a mechanism for learning skilled neuroprosthetic control of an artificial actual by forming a sensory representation of the actuator and its relationship to the body over time. The paradigm described in Chapter 3, in which chronic recording arrays are implanted in areas M1 and PMv simultaneously, could provide an ideal framework for testing these questions in future studies. Using the receptive field mapping procedure developed here, sensory responses of individual neurons could be tracked over periods of days or weeks as a subject practiced BMI control. Specifically, areas around the controlled actuator could be tested to see if sensory responses develop as control improves.

7.2.3 Causes of inter-subject variability in adaptation strategies for a constant velocity perturbation

The data presented in Chapter 4 show inconsistent responses to the same perturbation across subjects and control contexts. From the available data, it is not clear precisely which factors underlie these differences. In order to establish the constant velocity perturbation as a useful paradigm for studying questions of motor learning and adaptation, further efforts should be made to control for sources of variability such that consistent and predictable adaptation responses may be observed.

7.2.4 Advantages and disadvantages of building redundancy into applied BMI systems

Chapter 5 presented evidence that subjects are capable of utilizing more than the minimum required number of degrees of freedom in a neuroprosthetic actuator when these degrees of freedom are built into the system. However, the study did not establish whether allowing such redundant control would confer an advantage over typical non-redundant BMI paradigms. While redundancy may allow a greater range of function and potentially increased generalizability across different types of movements, it may be that the increased burden of control generated by increasing the number of controlled parameters is not worth the tradeoff in applied BMI systems. A controlled performance comparison between redundant and non-redundant BMI systems for a variety of decoding algorithms and task types should be performed in order to answer this question.

7.3 Conclusion

BMI holds great promise both as a treatment for motor impairments and as a platform for understanding brain function. Though much progress has been made, many details remain to be explored in order to fully realize either of these functions for this technology. This work has addressed a range of questions related to the design and implementation of BMI systems, as well as the control strategies employed by the brain during various types of BMI control. It has laid the groundwork for several future studies to investigate the performance effects of characteristics such as PMv control and redundancy. It has also established new paradigms for studying learning in the context of BMI control and potentially motor control in general.

8 Bibliography

Atkins DJ, Heard D, Donovan WH (1996) Epidemiologic Overview of Individuals with Upper-Limb Loss and Their Reported Research Priorities. J Prosthetics Orthot 8:2–11.

Berger DJ, Gentner R, Edmunds T, Pai DK, d' Avella A (2013) Differences in Adaptation Rates after Virtual Surgeries Provide Direct Evidence for Modularity. J Neurosci 33:12384–12394.

Biddiss E, Chau T (2007) Upper-Limb Prosthetics: Critical Factors in Device Abandonment. Am J Phys Med Rehabil 86:977–987.

Botvinick M, Cohen J (1998) Rubber hands "feel" touch that eyes see. Nature 391:756.

Burdick JW (1989) On the Inverse Kinematics of Redundant Manipulators: Characterization of the Self-Motion Manifolds. In: Advanced Robotics: 1989 (Waldron KJ, ed), pp 25–34.

Caggiano V, Fogassi L, Rizzolatti G, Thier P, Casile A (2009) Mirror Neurons Differentially Encode the Peripersonal and Extrapersonal Space of Monkeys. Science 324:403 –406.

Carmena JM (2013) Advances in Neuroprosthetic Learning and Control. Plos Biol 11:e1001561.

Carmena JM, Lebedev MA, Crist RE, O'Doherty JE, Santucci DM, Dimitrov DF, Patil PG, Henriquez CS, Nicolelis MAL (2003) Learning to Control a Brain–Machine Interface for Reaching and Grasping by Primates. Plos Biol 1:e42.

Carruthers G (2008) Types of body representation and the sense of embodiment. Conscious Cogn 17:1302–1316.

Chapin JK, Moxon KA, Markowitz RS, Nicolelis MAL (1999) Real-time control of a robot arm using simultaneously recorded neurons in the motor cortex. Nat Neurosci 2:664–670.

Collinger JL, Wodlinger B, Downey JE, Wang W, Tyler-Kabara EC, Weber DJ, McMorland AJ, Velliste M, Boninger ML, Schwartz AB (2013) High-performance neuroprosthetic control by an individual with tetraplegia. The Lancet 381:557 – 564.

Corke P (2011) Robotics, Vision and Control: Fundamental Algorithms in MATLAB. Springer Science & Business Media.

Crossley MJ, Fan JL, Ivry RB (2015) Unique Movements Lead to Independent Motor Memories for Visuomotor Adaptation. Prep.

Cunningham JP, Nuyujukian P, Gilja V, Chestek CA, Ryu SI, Shenoy KV (2011) A closed-loop human simulator for investigating the role of feedback control in brain-machine interfaces. J Neurophysiol 105:1932–1949.

Dangi S, Gowda S, Moorman HG, Orsborn AL, So K, Shanechi M, Carmena JM (2014) Continuous Closed-Loop Decoder Adaptation with a Recursive Maximum Likelihood

Algorithm Allows for Rapid Performance Acquisition in Brain-Machine Interfaces. Neural Comput 26:1811–1839.

Dangi S, Orsborn AL, Moorman HG, Carmena JM (2013) Design and Analysis of Closed-Loop Decoder Adaptation Algorithms for Brain-Machine Interfaces. Neural Comput 25:1693–1731.

Danziger Z, Fishbach A, Mussa-Ivaldi FA (2009) Learning Algorithms for Human-Machine Interfaces. IEEE Trans Biomed Eng 56:1502–1511.

De Rugy A, Loeb GE, Carroll TJ (2012) Muscle Coordination Is Habitual Rather than Optimal. J Neurosci 32:7384–7391.

Ehrsson HH (2009) How many arms make a pair? Perceptual illusion of having an additional limb. Perception 38:310–312.

Ehrsson HH, Spence C, Passingham RE (2004) That's My Hand! Activity in Premotor Cortex Reflects Feeling of Ownership of a Limb. Science 305:875–877.

Ethier C, Oby ER, Bauman MJ, Miller LE (2012) Restoration of grasp following paralysis through brain-controlled stimulation of muscles. Nature 485:368–371.

Fetz EE (1969) Operant Conditioning of Cortical Unit Activity. Science 163:955–958.

Fetz EE (2007) Volitional control of neural activity: implications for brain–computer interfaces. J Physiol 579:571–579.

Fetz EE, Baker MA (1973) Operantly conditioned patterns on precentral unit activity and correlated responses in adjacent cells and contralateral muscles. J Neurophysiol 36:179–204.

Fetz EE, Finocchio DV (1971) Operant Conditioning of Specific Patterns of Neural and Muscular Activity. Science 174:431–435.

Flash T, Hogan N (1985) The coordination of arm movements: an experimentally confirmed mathematical model. J Neurosci 5:1688–1703.

Fogassi L, Gallese V, Fadiga L, Luppino G, Matelli M, Rizzolatti G (1996) Coding of peripersonal space in inferior premotor cortex (area F4). J Neurophysiol 76:141 –157.

Gage GJ, Ludwig KA, Otto KJ, Ionides EL, Kipke DR (2005) Naïve coadaptive cortical control. J Neural Eng 2:52.

Ganguly K, Carmena JM (2009) Emergence of a Stable Cortical Map for Neuroprosthetic Control. Plos Biol 7:e1000153.

Ganguly K, Carmena JM (2010) Neural Correlates of Skill Acquisition with a Cortical Brain–Machine Interface. J Mot Behav 42:355–360.

Ganguly K, Dimitrov DF, Wallis JD, Carmena JM (2011) Reversible large-scale modification of cortical networks during neuroprosthetic control. Nat Neurosci 14:662–667.

Gilja V, Nuyujukian P, Chestek CA, Cunningham JP, Yu BM, Fan JM, Churchland MM, Kaufman MT, Kao JC, Ryu SI, Shenoy KV (2012) A high-performance neural prosthesis enabled by control algorithm design. Nat Neurosci 15:1752–1757.

Gomez-Rodriguez M, Peters J, Hill J, Schölkopf B, Gharabaghi A, Grosse-Wentrup M (2011) Closing the sensorimotor loop: haptic feedback facilitates decoding of motor imagery. J Neural Eng 8:036005.

Gowda S, Orsborn AL, Overduin SA, Moorman HG, Carmena JM (2014) Designing Dynamical Properties of Brain-Machine Interfaces to Optimize Task-Specific Performance. IEEE Trans Neural Syst Rehabil Eng 22:911–920.

Graziano MSA, Hu XT, Gross CG (1997) Visuospatial Properties of Ventral Premotor Cortex. J Neurophysiol 77:2268–2292.

Green AM, Kalaska JF (2011) Learning to move machines with the mind. Trends Neurosci 34:61–75.

Hari R, Hänninen R, Mäkinen T, Jousmäki V, Forss N, Seppä M, Salonen O (1998) Three hands: fragmentation of human bodily awareness. Neurosci Lett 240:131–134.

Harris CM, Wolpert DM (1998) Signal-dependent noise determines motor planning. Nature 394:780–784.

Heliot R, Venkatraman S, Carmena JM (2010) Decoder remapping to counteract neuron loss in brain-machine interfaces. In: 2010 Annual International Conference of the IEEE Engineering in Medicine and Biology Society (EMBC), pp 1670–1673.

Hlustík P, Solodkin A, Noll C, Small SL (2004) Cortical plasticity during three-week motor skill learning. J Clin Neurophysiol Off Publ Am Electroencephalogr Soc 21:180–191.

Hochberg LR, Bacher D, Jarosiewicz B, Masse NY, Simeral JD, Vogel J, Haddadin S, Liu J, Cash SS, van der Smagt P, Donoghue JP (2012) Reach and grasp by people with tetraplegia using a neurally controlled robotic arm. Nature 485:372–375.

Hochberg LR, Serruya MD, Friehs GM, Mukand JA, Saleh M, Caplan A, Branner A, Chen D, Penn RD, Donoghue JP (2006) Neuronal ensemble control of prosthetic devices by a human with tetraplegia. Nature 442:164–171.

Howard IS, Wolpert DM, Franklin DW (2013) The effect of contextual cues on the encoding of motor memories. J Neurophysiol 109:2632–2644.

Iriki A, Tanaka M, Iwamura Y (1996) Coding of modified body schema during tool use by macaque postcentral neurones. Neuroreport 7:2325–2330.

Jarosiewicz B, Chase SM, Fraser GW, Velliste M, Kass RE, Schwartz AB (2008) Functional network reorganization during learning in a brain-computer interface paradigm. Proc Natl Acad Sci 105:19486–19491.

Jolliffe I (2005) Principal Component Analysis. In: Encyclopedia of Statistics in Behavioral Science. John Wiley & Sons, Ltd.

Karni A, Meyer G, Jezzard P, Adams MM, Turner R, Ungerleider LG (1995) Functional MRI evidence for adult motor cortex plasticity during motor skill learning. Nature 377:155–158.

Kim S-P, Simeral JD, Hochberg LR, Donoghue JP, Black MJ (2008) Neural control of computer cursor velocity by decoding motor cortical spiking activity in humans with tetraplegia. J Neural Eng 5:455.

Kleim JA, Barbay S, Nudo RJ (1998) Functional Reorganization of the Rat Motor Cortex Following Motor Skill Learning. J Neurophysiol 80:3321–3325.

Kleim JA, Hogg TM, VandenBerg PM, Cooper NR, Bruneau R, Remple M (2004) Cortical Synaptogenesis and Motor Map Reorganization Occur during Late, But Not Early, Phase of Motor Skill Learning. J Neurosci 24:628–633.

Koralek AC, Costa RM, Carmena JM (2013) Temporally Precise Cell-Specific Coherence Develops in Corticostriatal Networks during Learning. Neuron 79:865–872.

Koralek AC, Jin X, Long Ii JD, Costa RM, Carmena JM (2012) Corticostriatal plasticity is necessary for learning intentional neuroprosthetic skills. Nature 483:331–335.

Koyama S, Chase SM, Whitford AS, Velliste M, Schwartz AB, Kass RE (2009) Comparison of brain–computer interface decoding algorithms in open-loop and closed-loop control. J Comput Neurosci 29:73–87.

Krakauer JW, Mazzoni P (2011) Human sensorimotor learning: adaptation, skill, and beyond. Curr Opin Neurobiol 21:636–644.

Krakauer JW, Pine ZM, Ghilardi M-F, Ghez C (2000) Learning of Visuomotor Transformations for Vectorial Planning of Reaching Trajectories. J Neurosci 20:8916–8924.

Li C-SR, Padoa-Schioppa C, Bizzi E (2001) Neuronal Correlates of Motor Performance and Motor Learning in the Primary Motor Cortex of Monkeys Adapting to an External Force Field. Neuron 30:593–607.

Li Z, O'Doherty JE, Hanson TL, Lebedev MA, Henriquez CS, Nicolelis MAL (2009) Unscented Kalman Filter for Brain-Machine Interfaces. Plos One 4.

Li Z, O'Doherty JE, Lebedev MA, Nicolelis MAL (2011) Adaptive Decoding for Brain-Machine Interfaces Through Bayesian Parameter Updates. Neural Comput 23:3162–3204.

Liu X, Mosier KM, Mussa-Ivaldi FA, Casadio M, Scheidt RA (2011) Reorganization of Finger Coordination Patterns During Adaptation to Rotation and Scaling of a Newly Learned Sensorimotor Transformation. J Neurophysiol 105:454–473.

Liu X, Scheidt RA (2008) Contributions of Online Visual Feedback to the Learning and Generalization of Novel Finger Coordination Patterns. J Neurophysiol 99:2546–2557.

Mahmoudi B, Sanchez JC (2011) A Symbiotic Brain-Machine Interface through Value-Based Decision Making. Plos One 6.

Matelli M, Luppino G, Rizzolatti G (1985) Patterns of cytochrome oxidase activity in the frontal agranular cortex of the macaque monkey. Behav Brain Res 18:125–136.

Moritz CT, Fetz EE (2011) Volitional control of single cortical neurons in a brain–machine interface. J Neural Eng 8:025017.

Moritz CT, Perlmutter SI, Fetz EE (2008) Direct control of paralysed muscles by cortical neurons. Nature 456:639–642.

Mosier KM, Scheidt RA, Acosta S, Mussa-Ivaldi FA (2005) Remapping Hand Movements in a Novel Geometrical Environment. J Neurophysiol 94:4362–4372.

Musallam S, Corneil BD, Greger B, Scherberger H, Andersen RA (2004) Cognitive Control Signals for Neural Prosthetics. Science 305:258–262.

Mussa-Ivaldi FA, Casadio M, Danziger ZC, Mosier KM, Scheidt RA (2011) Sensory motor remapping of space in human–machine interfaces. Prog Brain Res 191:45–64.

Nudo RJ, Milliken GW, Jenkins WM, Merzenich MM (1996) Use-dependent alterations of movement representations in primary motor cortex of adult squirrel monkeys. J Neurosci 16:785–807.

O'Doherty JE, Lebedev MA, Hanson TL, Fitzsimmons NA, Nicolelis MAL (2009) A Brain-Machine Interface Instructed by Direct Intracortical Microstimulation. Front Integr Neurosci 3 Available at: http://www.ncbi.nlm.nih.gov/pmc/articles/PMC2741294/ [Accessed April 10, 2015].

O'Doherty JE, Lebedev MA, Ifft PJ, Zhuang KZ, Shokur S, Bleuler H, Nicolelis MAL (2011) Active tactile exploration using a brain-machine-brain interface. Nature 479:228–231.

Orsborn AL, Dangi S, Moorman HG, Carmena JM (2011) Exploring time-scales of closed-loop decoder adaptation in brain-machine interfaces. Conf Proc Annu Int Conf IEEE Eng Med Biol Soc IEEE Eng Med Biol Soc Conf 2011:5436–5439.

Orsborn AL, Dangi S, Moorman HG, Carmena JM (2012) Closed-loop decoder adaptation on intermediate time-scales facilitates rapid BMI performance improvements independent of decoder initialization conditions. IEEE Trans Neural Syst Rehabil Eng 20:468–477.

Orsborn AL, Moorman HG, Overduin SA, Shanechi MM, Dimitrov DF, Carmena JM (2014) Closed-Loop Decoder Adaptation Shapes Neural Plasticity for Skillful Neuroprosthetic Control. Neuron 82:1380–1393.

Pearson KG (1993) Common Principles of Motor Control in Vertebrates and Invertebrates. Annu Rev Neurosci 16:265–297.

Ranganathan R, Adewuyi A, Mussa-Ivaldi FA (2013) Learning to be Lazy: Exploiting Redundancy in a Novel Task to Minimize Movement-Related Effort. J Neurosci 33:2754–2760.

Ranganathan R, Wieser J, Mosier KM, Mussa-Ivaldi FA, Scheidt RA (2014) Learning Redundant Motor Tasks with and without Overlapping Dimensions: Facilitation and Interference Effects. J Neurosci 34:8289–8299.

Rioult-Pedotti MS, Friedman D, Donoghue JP (2000) Learning-induced LTP in neocortex. Science 290:533–536.

Rizzolatti G, Camarda R, Fogassi L, Gentilucci M, Luppino G, Matelli M (1988) Functional organization of inferior area 6 in the macaque monkey. Exp Brain Res 71:491–507.

Sanchez-Vives MV, Spanlang B, Frisoli A, Bergamasco M, Slater M (2010) Virtual Hand Illusion Induced by Visuomotor Correlations. Plos One 5:e10381.

Santello M, Flanders M, Soechting JF (1998) Postural Hand Synergies for Tool Use. J Neurosci 18:10105–10115.

Santhanam G, Ryu SI, Yu BM, Afshar A, Shenoy KV (2006) A high-performance brain–computer interface. Nature 442:195–198.

Scholz JP, Schöner G (1999) The uncontrolled manifold concept: identifying control variables for a functional task. Exp Brain Res 126:289–306.

Scott SH (2003) The role of primary motor cortex in goal-directed movements: insights from neurophysiological studies on non-human primates. Curr Opin Neurobiol 13:671–677.

Serruya MD, Hatsopoulos NG, Paninski L, Fellows MR, Donoghue JP (2002) Brain-machine interface: Instant neural control of a movement signal. Nature 416:141–142.

Shanechi MM, Carmena JM (2013) Optimal feedback-controlled point process decoder for adaptation and assisted training in brain-machine interfaces. In: 2013 6th International IEEE/EMBS Conference on Neural Engineering (NER), pp 653–656.

Shanechi MM, Orsborn AL, Moorman HG, Gowda S, Dangi S, Carmena JM (2015) Rapid control and feedback rates in the sensorimotor pathway enhance neuroprosthetic control. Prep.

Shpigelman L, Lalazar H, Vaadia E (2009) Kernel-ARMA for Hand Tracking and Brain-Machine interfacing During 3D Motor Control. In: Advances in Neural Information Processing Systems 21 (Koller D, Schuurmans D, Bengio Y, Bottou L, eds), pp 1489–1496. Curran Associates, Inc.

Slater M, Perez-Marcos D, Ehrsson HH, Sanchez-Vives MV (2008) Towards a Digital Body: The Virtual Arm Illusion. Front Hum Neurosci 2 Available at: http://www.ncbi.nlm.nih.gov/pmc/articles/PMC2572198/ [Accessed July 9, 2013].

Slifkin AB, Vaillancourt DE, Newell KM (2000) Intermittency in the Control of Continuous Force Production. J Neurophysiol 84:1708–1718.

So K, Dangi S, Orsborn AL, Gastpar MC, Carmena JM (2014) Subject-specific modulation of local field potential spectral power during brain-machine interface control in primates. J Neural Eng 11:026002.

Sosnoff JJ, Newell KM (2005) Intermittent visual information and the multiple time scales of visual motor control of continuous isometric force production. Percept Psychophys 67:335–344.

Suminski AJ, Tkach DC, Fagg AH, Hatsopoulos NG (2010) Incorporating Feedback from Multiple Sensory Modalities Enhances Brain-Machine Interface Control. J Neurosci 30:16777–16787.

Taylor DM, Tillery SIH, Schwartz AB (2002) Direct Cortical Control of 3D Neuroprosthetic Devices. Science 296:1829–1832.

Todorov E, Jordan MI (2002) Optimal feedback control as a theory of motor coordination. Nat Neurosci 5:1226–1235.

Tresch MC, Jarc A (2009) The case for and against muscle synergies. Curr Opin Neurobiol 19:601–607.

Tsakiris M, Carpenter L, James D, Fotopoulou A (2010) Hands only illusion: multisensory integration elicits sense of ownership for body parts but not for non-corporeal objects. Exp Brain Res Exp Hirnforsch Expérimentation Cérébrale 204:343–352.

Uno Y, Kawato M, Suzuki R (1989) Formation and control of optimal trajectory in human multijoint arm movement. Minimum torque-change model. Biol Cybern 61:89–101.

Velliste M, Perel S, Spalding MC, Whitford AS, Schwartz AB (2008) Cortical control of a prosthetic arm for self-feeding. Nature 453:1098–1101.

Vidaurre C, Sannelli C, Müller K-R, Blankertz B (2010) Machine-Learning-Based Coadaptive Calibration for Brain-Computer Interfaces. Neural Comput 23:791–816.

Wahnoun R, He J, Tillery SIH (2006) Selection and parameterization of cortical neurons for neuroprosthetic control. J Neural Eng 3:162.

Wander JD, Blakely T, Miller KJ, Weaver KE, Johnson LA, Olson JD, Fetz EE, Rao RPN, Ojemann JG (2013) Distributed cortical adaptation during learning of a brain–computer interface task. Proc Natl Acad Sci 110:10818–10823.

Wodlinger B, Downey JE, Tyler-Kabara EC, Schwartz AB, Boninger ML, Collinger JL (2015) Ten-dimensional anthropomorphic arm control in a human brain−machine interface: difficulties, solutions, and limitations. J Neural Eng 12:016011.

Wolpert DM, Diedrichsen J, Flanagan JR (2011) Principles of sensorimotor learning. Nat Rev Neurosci 12:739–751.

Wu W, Gao Y, Bienenstock E, Donoghue JP, Black MJ (2006) Bayesian Population Decoding of Motor Cortical Activity Using a Kalman Filter. Neural Comput 18:80–118.

Wu W, Shaikhouni A, Donoghue JP, Black MJ (2004) Closed-loop neural control of cursor motion using a Kalman filter. In: 26th Annual International Conference of the IEEE Engineering in Medicine and Biology Society, 2004. IEMBS '04, pp 4126–4129.